



**Michigan
Technological
University**

Michigan Technological University
Digital Commons @ Michigan Tech

Dissertations, Master's Theses and Master's Reports

2022

CHARACTERIZATION OF HYDRAULIC FLOW NOISE INDUCED BY SPOOL VALVES

Carter A. Paprocki

Michigan Technological University, capaproc@mtu.edu

Copyright 2022 Carter A. Paprocki

Recommended Citation

Paprocki, Carter A., "CHARACTERIZATION OF HYDRAULIC FLOW NOISE INDUCED BY SPOOL VALVES",
Open Access Master's Thesis, Michigan Technological University, 2022.
<https://doi.org/10.37099/mtu.dc.etr/1446>

Follow this and additional works at: <https://digitalcommons.mtu.edu/etr>



Part of the [Acoustics, Dynamics, and Controls Commons](#)

CHARACTERIZATION OF HYDRAULIC FLOW NOISE INDUCED BY SPOOL
VALVES

By

Carter A. Paprocki

A THESIS

Submitted in partial fulfillment of the requirements for the degree of

MASTER OF SCIENCE

In Mechanical Engineering

MICHIGAN TECHNOLOGICAL UNIVERSITY

2022

© 2022 Carter A. Paprocki

This thesis has been approved in partial fulfillment of the requirements for the Degree of MASTER OF SCIENCE in Mechanical Engineering.

Department of Mechanical Engineering -Engineering Mechanics

Thesis Co-Advisor: *Andrew Barnard*

Thesis Co-Advisor: *Vijaya V. N. Sriram Malladi*

Committee Member: *Jason Blough*

Department Chair: *Jason Blough*

Table of Contents

List of Figures	iv
List of Tables	vi
Acknowledgments.....	vii
Abstract.....	viii
1 Introduction.....	1
1.1 Motivation	2
1.2 Project Deliverables	3
1.3 Background	4
1.3.1 Types of Noise	5
1.3.2 Piston Pump.....	9
2 Methods and Materials.....	13
2.1 Purpose	13
2.2 Accessory Drive Layout.....	13
2.3 Hydraulic Oil Selection	15
2.4 Accessory Drive Test Plan	16
2.4.1 Control Variables.....	21
2.4.2 Dependent Variables	22
2.5 Sound Enclosure.....	23
2.6 Brake Valve Circuit.....	27
2.6.1 Fixture Design.....	29
2.6.2 Brake Valve Test Plan	32
2.6.3 Brake Valve Control Variables.....	33
2.6.4 Brake Valve Dependent Variables.....	34
2.6.5 Fixture Modal Validation.....	35
3 Results.....	38
3.1 Accessory Valve Results	38
3.2 Brake Valve Results	42
3.2.1 Valve Sensors.....	45
3.2.2 Orifice Sensors.....	52
3.2.3 Valve Flow Regions.....	56
3.2.4 Quantifying Flow Region Energy	62
3.2.5 Dynamic Parameter Evolution Through Testing	66
4 Conclusion	72
5 Reference List	76

List of Figures

Figure 1-1: The cross-section of an inline pump.....	9
Figure 1-2: Inline pump drive mechanism.....	10
Figure 2-1: Accessory valve system layout	15
Figure 2-2: Sensor locations for accessory valve hydraulic circuit.....	23
Figure 2-3: The acoustic enclosure design	24
Figure 2-4: Acoustic sound enclosure for the electric motor. Closed-cell Sounddown foam cladded the interior	24
Figure 2-5: The known and unknown sources are shown in position for the test.	25
Figure 2-6: Sound enclosure noise reduction.	26
Figure 2-7: Brake Valve circuit major components and layout.....	28
Figure 2-8: Brake valve platform. With string pot bracket.. ..	30
Figure 2-9: Mounted slack adjusters and the construction of mount.....	31
Figure 2-10: Brake Valve Sensor Location Diagram.....	34
Figure 2-11: Coordinate cube representing accelerometer mounting location.. .	35
Figure 2-12: H1 FRF for valve frame excitation.....	36
Figure 3-1: Accessory Valve fluid borne Noise at 1000 rpm.....	38
Figure 3-2: Drive Motor impact on Flow Noise.....	39
Figure 3-3: Valve spring Root Cause Analysis... ..	40
Figure 3-4: Valve flow regions are identified with the colored region.....	43
Figure 3-5: Overlay of all displacement measurements, showing the phase relation of components.	44
Figure 3-6: Operation temperature is taken for the system during valve operation.....	46
Figure 3-7: Spectrogram of valve opening. Most flow noise is limited to region 3 with increased dynamic pressure on outlet ports... ..	47
Figure 3-8: Valve Excitation regions.	49
Figure 3-9: Frequency-based PSD looking at the energy response of the four- valve ports... ..	48
Figure 3-10: Time-based PSD for inlet and outlet ports correlated to brake spool displacement.....	49
Figure 3-11: Acoustic Identification of mechanical clunk... ..	50

Figure 3-12: Comparison of Broadband dynamic pressure between orifices..	52
Figure 3-13: Orifice PSD in the time domain. The possible whistle narrowband responses have been identified...	53
Figure 3-14: Orifice PSD in the time domain. They mirror the dynamic pressure signals on the outlet ports of the valve.....	54
Figure 3-15: The four indices described are plotted on a flowrate plot...	56
Figure 3-16: Flow regions overlaid with flow rate derivation...	57
Figure 3-17: Correlation of flow rate to the region of the brake spool.....	58
Figure 3-18: The black curve is the accumulator static pressure supplying oil to the valve, with the red curves being the outlet pressure of the valve.....	59
Figure 3-19: Acoustic energy compared to the flow rate of the valve...	60
Figure 3-20: Top dynamic pressure sensor power comparison for inlet and outlet valve ports...	62
Figure 3-21: Bottom dynamic pressure sensor power comparison for inlet and outlet valve ports.....	62
Figure 3-22: Accelerometer Power measured in three-axis for each flow region...	63
Figure 3-23: Microphone SEL during fast pedal sweep...	65
Figure 3-24: Heatmap of the dataset for normalized microphone pressure level...	66
Figure 3-25: Heatmap of the dataset for normalized top inlet dynamic pressure level..	67
Figure 3-26: Heatmap of the dataset for normalized top outlet dynamic pressure level...	68
Figure 3-27: Heatmap of the dataset for normalized Acceleration X...	69
Figure 3-28: Heatmap of the dataset for normalized Acceleration Y...	69
Figure 3-29: Heatmap of the dataset for normalized Acceleration Z.....	70

List of Tables

Table 2.1 Chevron Rando HDZ 32 physical Properties. Error! Bookmark not defined.	16
Table 2.2 Expansion chamber boundary condition Test Plan.....	17
Table 2.3 4-meter-hose boundary condition test Plan.	18
Table 2.4 Static valve position test plan with 4-meter-hose.....	18
Table 2.5 Static valve position test plan with Expansion Chamber.....	19
Table 2.6: Root cause testing for accessory valve shock events.....	21
Table 2.7: Whoosh valve test procedure..	33

Acknowledgments

I want to begin by thanking my two co-advisors, Andrew Barnard and Sriram Malladi, for supporting me and guiding me through the process of my Master's research. Their support and guidance allowed me to evolve my skills as an engineer and researcher more than I had previously thought possible. I would also like to thank my contacts at Caterpillar Inc., Sarah Nelson, Ed Mate, Michael Sorokin, David Copley, and Ryan Stoffel, for their years of knowledge and experience. Furthermore, I'd like to thank Mike Johnson and the whole team of Caterpillar Global Sound Solutions for the opportunity to work on this project and build my skills. Next, I would like to thank Michigan Technological University for the support and lab facilities that allowed this project to happen and for the years of world-leading education. Last but not least, I would like to thank my girlfriend, Rachael, along with all of my friends and family who supported me.

Abstract

The purpose of the hydraulic flow noise research was to investigate the relationship between operational valve parameters and flow noise generation.

The primary consideration was correlating the flow noise generated by the valve with the distinct valve open positions. This data would allow future valve designs to account for features that cause increased flow noise and move those features away from high flow valve displacements. By implementing this, companies would be able to design quieter hydraulic systems that will not expose operators to undesirable sound quality present from the hydraulic actuation of the valve.

The experiments were conducted using two valves with different internal geometry and comparing the flow noise's excitation and acoustic energy. Using a controlled closed circuit valve system, the fluid-born noise could be isolated from the pump harmonics and background noise to develop accurate flow noise profiles for the valves under various operating conditions. In the future, more valves could be tested to create a more robust profile library using the test methods developed.

1 Introduction

In today's heavy machinery, great strides have been made to limit the noise generated by the engine and other components of the machine. This has caused acoustic sources such as hydraulic pumps and valve circuits that were not noticeable in previous iterations to be some of the most significant source of noise in current production models. The use of these hydraulic circuits is widespread in the industry because of their small footprint and the ability to quickly transfer power from the main power unit to anywhere on the machine. These advancements, paired with the OSHA standard 1910.95 - Occupational noise exposure, have shifted the focus of noise control research from the traditional sources such as the engine and drive train to prioritize limiting the radiation of hydraulic noise from the machine [11].

Furthermore, the competitiveness of the heavy machinery market-space has closed the gap to where small changes in perceived noise levels and noise profiles of hydraulic components are now scrutinized. Because of this understanding, the noise profile of different valve geometries and the interaction with fluid must be understood. Current methods require long testing on the machine, which struggles to provide the cleanest data. During in field testing, the vehicle's powertrain interferes with the airborne sound measurement and makes the data acquisition and processing difficult, this research aims to characterize

the valve in a laboratory setting to allow a better understanding of the system behavior.

Also, the rigid structure of the machine frame paired with having most hydraulic components being mounted directly to the machine frame, due to machine packaging and space limitations, this ultimately increases the potential of sound radiation to be transferred from the hydraulic components to the frame. The purpose of the testing was to understand the sound quality generated by the hydraulic spool valve under laboratory settings and correlate them to on-machine testing.

1.1 Motivation

This research will help engineers of off-highway heavy machinery to develop hydraulic valves that will not impede the operator from working all day and stay more focused on the task at hand. This would also allow them to have increased situational awareness, allowing improvements to the worksite to reduce worker fatigue which may be caused by noise. With the research focused on the brake valve, which is required to be rigidly mounted to the floor of the operator cab, it transmits some of the brakes vibro-acoustic signature into the cab and may cause additional fatigue which could lead to affecting the operators driving experience. Once this signature is fully understood steps can be taken on the valves design to mitigate the undesired noise profile.

Through experimentation, the noise profile can be characterized and linked back to CFD modeling allowing for high fidelity models to predict the valve spool behavior and noise profile. Current methods are time-consuming and have higher noise contaminations; this could be circumvented by using an experimentally derived model that could predict the noise generated using an easily measured parameter on the machine. This research aims to develop a way to characterize hydraulic flow noise profiles using readily available variables and then predict the noise levels of the valve under various operating conditions. [4]

The experiment further evaluated the findings of a previous graduate students work and aimed to develop a new valve circuit. This test bench could be evaluated using the same methods as the previous test bench and ascertain how the valve vibro-acoustic signature changes due to different internal geometry and system parameters. The conclusions found using these test parameters will then be used to decrease the valve noise levels and create better test methods to evaluate new designs. [1]

1.2 Project Deliverables

Accessory Valve Circuit

- 1. Understand the different valve interaction regions and their effect on flow noise.**
- 2. Determine the difference in valve behavior under various loading parameters.**
- 3. Identify the effect of boundary conditions on the flow noise.**

Brake Valve Circuit

- 1. Identify Spool valve positions and correlate them to flow characteristics.**
- 2. Understand the difference in noise generation off the machine and correlate it to on-machine tests.**
- 3. Characterize the energy created by the fluid moving through the valve.**

1.3 Background

Hydraulics can be classified as any system that uses pressurized fluid such as liquid or gas to provide power, control action, or convert rotational work to other forms. The use of hydraulics as compact mechanical systems proliferated in the 20th century. They became less complicated and cheaper than traditional mechanical linkages. [3]

A key advantage of hydraulic systems was creating linear movement from simple hydraulic pistons. Using a linear application of pressure, the system can actuate implements found on off-road machinery through the use of pressure differential cylinders. Comparing this to mechanical and electrical systems, which have extra components to do the same task, [4] hydraulic systems also operated with less maintenance than their electromechanical counterparts. As the machine power demand grew, machine performance has required parts to become smaller, and lighter. This decrease in mass and has caused the noise generated to increase due to the components radiate more energy due to the flow cavitation. This in turn creates more structure interaction, and acoustic radiation. The nature of acoustic research is difficult due to the complex interaction of other noise sources present in the test bench. Because of this complexity, understanding how the fluid interacts with the internal geometry of the valve will allow minor changes to be made to the design.

1.3.1 Types of Noise

The majority of hydraulic noise can be traced to the hydraulic pump, coupled to machine power plant to provide pressure to the circuit. The reason pump noise is not under the scope of this research is because the pump has a very different acoustic signature when compared to the valve. The pump is periodic which is easily understood and mitigated using traditional methods. Valves however have

to be placed at specific junctions which can be near the operator and can often dynamically excite the structure it is mounted to. For the two valves tested in the experiment, the accessory drive valve has high pressure hydraulic fluid moving through the valve body which is very difficult to predict and understand. For the brake pedal valve, its placement in the cab floor can make any hydraulic noise it generates particularly audible to the operator. This flow noise increases the sound exposure level experienced by the operator, ultimately increasing operator fatigue and in some instances leading to operator discomfort. [2]

Fluid Borne Noise

Fluid-borne noise is predominantly radiated by the interaction of a turbulent fluid with the boundary of the solid structure, which in turn cause excitation of the structure and end up producing higher airborne noise levels. This increased acoustic noise level is sometimes due to the hydraulic lines running across many of the machine's body panels which could act as large acoustic radiators. The energy is then transferred from the flow noise into the structure. Not only is the increased valve noise detrimental to the perceived acoustic levels, but over time it could also fatigue certain parts of the structure through vibrational energy.

While many things can create hydraulic flow noise, a main component is the pressure ripple generated by the valve as it opens. The moving spool creates a large pressure gradient across a small channel in the valve, which can induce

cavitation. A different type of contributor to hydraulic noise is the pump harmonics generated by the inline piston pump. The pump will excite specific frequencies, which could be transmitted into a structure, especially if that structure shares a natural frequency with the pump harmonics. [3]

With the scope of the project focused on understanding the causes of valve noise, its focus was placed on the parameters that caused flow noise instead of how flow noise transfers into other structures or mediums. Through this lens, the flow noise was analyzed, considering the main contributors to fluid-borne noise such as cavitation, instability in fluid flow, and impact of valve components or fluid. Cavitation is often the most significant contributor to valve flow noise; and can be described as thousands of tiny low-pressure gas bubbles formed by edges in the valve and spool. After these low-pressure bubbles form, they will move downstream, recompress to liquid, creating a significant broadband shock signal as they collapse. [3] This phenomenon is common in the pressure regulating valves due to the spool needing to restrict the fluid's path. It is believed that the turbulent low-pressure zone behind the valve metering geometry contributes to flow noise. The outgassing of the fluid is produced in the discharge pipe of the valve due to the significant pressure drop in this transition region. Outgassing is the process of dissolved air returning to the gaseous state once the pressure drops below the critical saturation pressure. It should be noted that cavitation can create large amounts of energy from the collapse of the bubbles in

a small amount of time. Because of this, if the cavitation occurs at a boundary of a solid surface, it can damage the material causing fatigue and pitting; this high level of stress can wear components quickly. On the contrary, when the bubbles collapse with fluid surrounding them, the energy is transferred to fluid-borne noise. [3] The easiest way to combat valve cavitation is to create a laminar flow that does not create large pressure drops across the valve surface geometry.

Airborne Noise

Airborne noise is the energy that is effectively transmitted from the fluid and structure and radiates into the air. The distinction between structure-borne noise, fluid-borne noise, and airborne noise can be difficult to understand at first because, in the end, operators mainly experience airborne noise. An easy way to understand the difference is through a common approach used by acoustic engineers of Source-Path-Receiver. The source of the noise is either the pump, valve, or fluid flow in the hydraulic lines, meaning that once the energy is created it then moves through a path such as solid structure, fluid, or directly to the air. [1] Then for all situations, the sound can be detected as airborne noise by the operator of the machine as the receiver. Using this method, a slight but necessary distinction can be formed. The distinction between the source, path, and receiver is important to effectively diagnose the energy transfer path through the entire system.

Many hydraulic airborne noise signatures are similar to the fluid-noise discussed above. They are tonal in nature and are driven by the pressure ripple of the pump through the fluid. Next, the main component is broadband sound generated by the valve cavitation. This is predominantly found as the valve opens but quickly stops once the pressure differential between the inlet and outlet ports of the valve have equalized and flow has stopped.

1.3.2 Piston Pump

The pump used in this experiment was a nine-piston inline pump. This style of pump is characterized by a central driveshaft that moves the pistons up and down in each cylinder to pump the fluid. It is then connected to an inclined swashplate, that when it rotates the pistons move and push fluid from the pump. On the top of the piston ports is a plate that allows fluid to flow into the pump, and then the port switches when the crank has moved 180 degrees from top dead center and when the piston is at its rearmost position as seen in Figure 2. Then the pump plate will move to the discharge port allowing the flow to be pressurized and flow through the pump. The described positions and components of an inline piston pump can be seen in figure 1. [3]

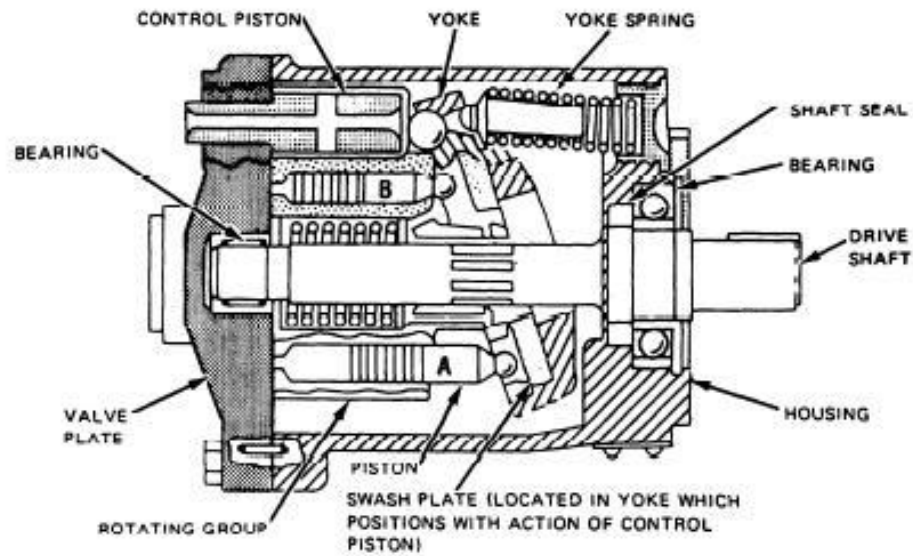


Figure 4-13.—In-line axial piston pump.

Figure 1-1: The cross-section of an inline pump. [8]

Overall the main advantage of the inline piston pump is that it can create a smooth pressure flow when compared to other geometries. Also, the pump is designed with an internal pressure relief stroke back screw. This means that it is able to change the operating pressure with minimal effects on flow rate. This gives the valve a consistent operating pressure to flow and drive the different components on the machine.

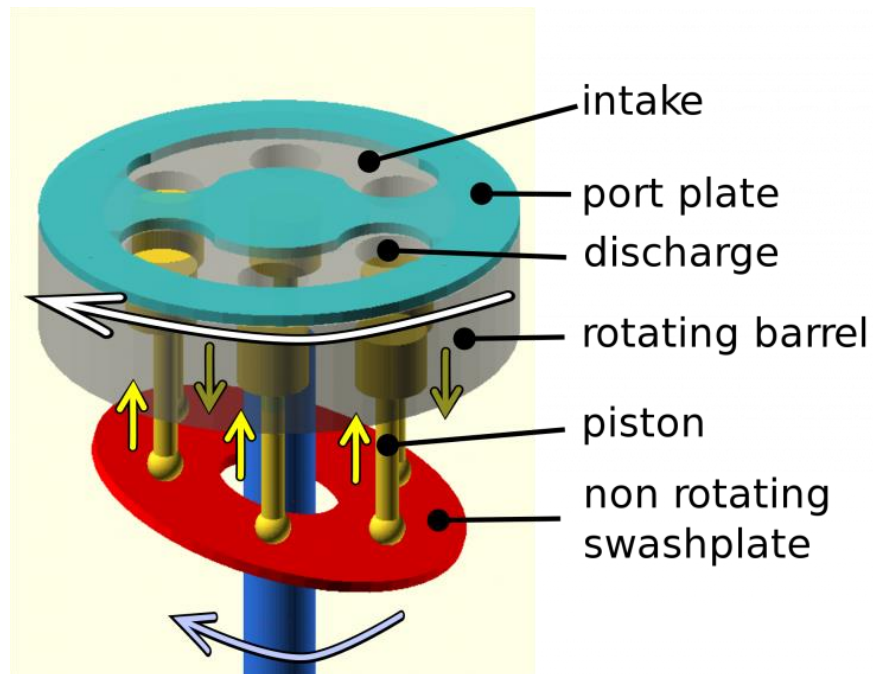


Figure 1-2: Inline pump drive mechanism. [7]

Pump Harmonics

It is the release of the pressure built up in each of the pistons that creates a ripple in the flow. This ripple is detrimental to the valve noise research because it adds energy to the dynamic pressure sensor signals. But the saw tooth pressure signal found in the ripple can be filtered out during data post-processing to more clearly see a flow cavitation signal in the hydraulic circuit. Piston pumps are a 1st order rotational machinery which means that for every rotation of the drive shaft the piston completes one oscillation. Since there are nine pistons on this pump design it is a 9th order piston pump, and these pistons move in a sinusoidal pattern and create a pressure ripple through the hydraulic fluid. This pressure

ripple paired with cavitation causes noise interaction with the solid structural components. [3]

$$Frequency [Hz] = \frac{(Order \#) \times RPM}{60} \quad (1)$$

2 Methods and Materials

2.1 Purpose

The purpose of the test bench was to lay out a repeatable system where the flow noise could be analyzed for two different types of hydraulic valves. The project's scope was split into two phases, with the first test bench designed to mimic the circuit for an accessory drive valve. The second test bench was designed to characterize the operation of a brake valve.

2.2 Accessory Drive Layout

The accessory valve test bench focused on characterizing the relationship between the valve's open valve area and the calculated flow noise. Open area of the valve is defined as the surface area of the port that allows the fluid to flow through the valve. During the testing of the accessory valve, it was discovered that the static pressure sensor required to measure pressure in the internal valve compensator affected the valve's response characteristics. The design of the valve required an auxiliary pressure regulator called a compensator to control the valves flow behavior. This compensator moves independently of any controllable input and proved to be extremely difficult to predict and characterize. The compensator needed a spring to buffer its movement, but the spring had to be removed when installing the sensor. The data collected is still applicable to the

research, but it was noted that the unknown open area of the compensator would cause an unforeseen unknown in the data analysis.

The system was powered by a 100-horsepower three-phase electric motor attached to an inline nine-piston pump. This pump was then connected to a pressure relief and pilot valve to prevent over-pressuring the system. The pilot valve provided an oil supply to the accessory valve to actuate the spool whose position is controlled by an electronic solenoid. The system's flow rate was controlled by manually manipulating spool position with a dial controller. Once the pressure was built up in the accessory valve, the main spool would begin to stabilize the flow rate while a tertiary compensator spool would regulate the outlet pressure of the valve. This complex internal geometry proved challenging to characterize a true open area of the valve. After the hydraulic fluid passes through the valve, the flow would enter one of two boundary conditions. These boundary conditions were tested to determine whether internal fluid modes would impact the flow-induced noise. One boundary condition selected is a four-meter hose; this was chosen to replicate the response for the valve actuating an implement far away from the valve's location. The second boundary condition was an expansion chamber; this allowed the fluid to immediately enter a large volume and drop the static outlet pressure. Immediately following the boundary condition was a needle valve set to specific back pressures to provide hydraulic loading on the system. In real-world hydraulic applications, the driven

implement's actuation provides the load. Once the fluid is finished moving through the system, it returns to the tank.

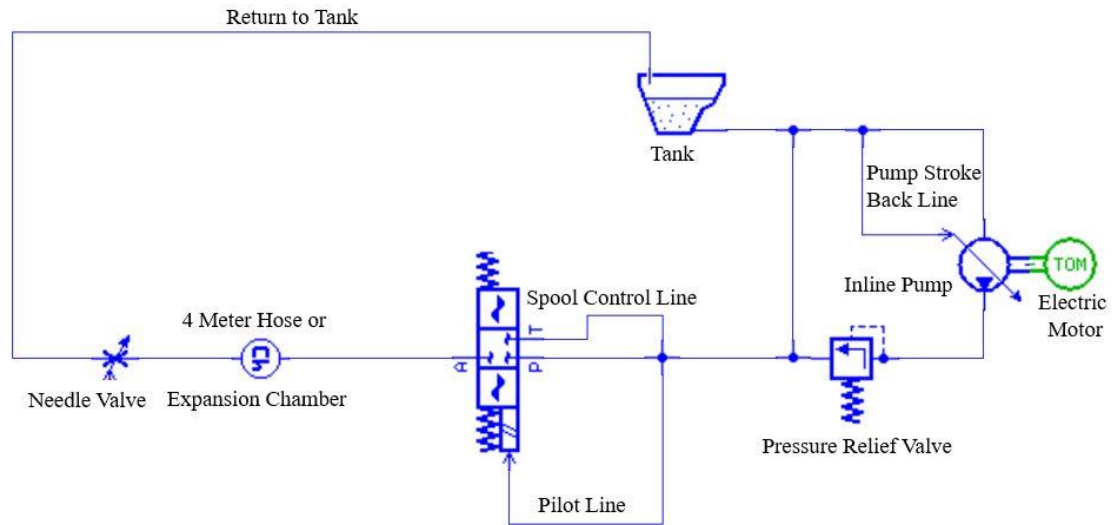


Figure 2-1: Accessory valve system layout.

2.3 Hydraulic Oil Selection

The hydraulic oil used in the test bench was Chevron Rando HDZ 32. Its properties were very similar to Cat®'s propriety oil, but this oil was available at MTU. The physical properties were also very advantageous for the test bench. The main concern regarding oil selection was its viscosity; due to the limitations of the MTU test bench, it was challenging to keep the oil at operating temperature. But, Rando's wide operating range offered very little change in

viscosity, allowing the system behavior to mimic those found in the field. Below the properties of interest to this research can be seen in table 2-1.

Table 2.1: Chevron Rando HDZ 32 physical Properties

	Density @ 15 °C [g/cc]	Viscosity 40 °C [cSt]	Viscosity 100 °C [cSt]	API Gravity	Bulk Modulus [kpsi]
Rando HDZ 32	0.8433	32	6.2	34	285

2.4 Accessory Drive Test Plan

Testing for the accessory valve was conducted in two parts, with the open area sweep data predominantly used for the data analysis, and the static data was used to validate sweep runs. The static data was collected with the valve spool position stationary at various positions. The main issue for the sweep runs was having the pump harmonics interfere with the desired flow noise. The hydraulic pump would create very high energy frequency bands that would be seen throughout the entire run. To counter this, it was chosen to do steady-state tests with the valve not changing position and remove the pump harmonics from the flow noise signature.

Table 2.2: Expansion chamber Test Plan.

Accessory Valve Sweep Test		
Motor Speed [RPM]	Backpressure [PSI]	Boundary Condition
1000	1000	Expansion Chamber
1000	1500	Expansion Chamber
1000	2000	Expansion Chamber
1500	1000	Expansion Chamber
1500	1500	Expansion Chamber
1500	2000	Expansion Chamber
2000	1000	Expansion Chamber
2000	1500	Expansion Chamber
2000	2000	Expansion Chamber

Table 2.3: 4-meter-hose boundary condition test Plan.

Accessory Valve Sweep Test		
Motor Speed [RPM]	Backpressure [PSI]	Boundary Condition
1000	1000	4 Meter Hose
1000	1500	4 Meter Hose
1000	2000	4 Meter Hose
1500	1000	4 Meter Hose
1500	1500	4 Meter Hose
1500	2000	4 Meter Hose
2000	1000	4 Meter Hose
2000	1500	4 Meter Hose
2000	2000	4 Meter Hose

Table 2.4: Static valve position test plan with 4-meter-hose.

Accessory Valve Static Test			
Motor Speed [RPM]	Backpressure [PSI]	Valve Position [mm]	Boundary Condition
1500	1500	2	4 Meter Hose
1500	1500	2.5	4 Meter Hose
1500	1500	3	4 Meter Hose
1500	1500	3.5	4 Meter Hose
1500	1500	4	4 Meter Hose

1500	1500	4.5	4 Meter Hose
1500	1500	5	4 Meter Hose
1500	1500	5.5	4 Meter Hose
1500	1500	6	4 Meter Hose
1500	1500	6.5	4 Meter Hose
1500	1500	7	4 Meter Hose
1500	1500	7.5	4 Meter Hose

Table 2.5: Static valve position test plan with Expansion Chamber.

Accessory Valve Static Test			
Motor Speed [RPM]	Backpressure [PSI]	Valve Position [mm]	Boundary Condition
1500	1500	2	Expansion Chamber
1500	1500	2.5	Expansion Chamber
1500	1500	3	Expansion Chamber
1500	1500	3.5	Expansion Chamber
1500	1500	4	Expansion Chamber
1500	1500	4.5	Expansion Chamber
1500	1500	5	Expansion Chamber

1500	1500	5.5	Expansion Chamber
1500	1500	6	Expansion Chamber
1500	1500	6.5	Expansion Chamber
1500	1500	7	Expansion Chamber
1500	1500	7.5	Expansion Chamber

During the data analysis, it was found that the accelerometers located near the compensator were being saturated due to a shock event. This prompted a new set of tests to identify whether the removal of the spring caused these events or if it occurred when the accessory valve was in its factory configuration. The spring had been removed to provide an access port for measuring the static pressure in the spool cavity, and the geometry of the spring would have interfered with the static pressure sensor diaphragm. By recording static pressure, the compensator position could be modeled, and then the total open area of the valve, with both the compensator and main spool, could be characterized. The tests shown in Table 2-6 were conducted to validate the removal of the spring as the root cause of the shock events. During the valve area sweeps, it was found that most overloads occurred at 2000 rpm motor speed and 1000 psi backpressure from the needle valve. It is believed that these parameters created the most dynamic response for the valve due to the low flow resistance downstream paired with the

maximum hydraulic flow coming from the hydraulic pump. Testing was done to determine if the spring changed the valves behavior and if the shock events were linked to the springs removal. It was found through this testing that the removal of the spring was the root cause of the compensator spools erratic behavior.

Table 2.6: Root cause testing for accessory valve shock events.

Accessory Valve Shock Test				
Motor Speed [RPM]	Backpressure [PSI]	Spring Installed	Boundary Condition	Overload
2000	1000	Yes	Expansion Chamber	Yes
2000	1000	Yes	Expansion Chamber	Yes
2000	1000	No	Expansion Chamber	No
2000	1000	No	Expansion Chamber	No

2.4.1 Control Variables

The three variables controlled during the testing were valve spool position, motor rpm, and system backpressure. The valve open area was the primary variable controlled because it directly correlated with the flow noise produced, and the

purpose of the experiment was to characterize the relation between the two. Next, the rpm was set to various values in the operating range of the machine power plant. The final control variable was the needle valve controlling backpressure; this allowed the valve to be tested under different load profiles as seen in the real-world application of the accessory drive valve.

2.4.2 Dependent Variables

To characterize the flow noise created by the accessory drive valve, 16 sensors were used to measure all variables that contribute to the propagation of flow-induced noise. The instrumentation for the accessory valve focused mainly on static pressure drops and dynamic pressure readings from across the valve on the inlet and outlet fittings. A microphone array was constructed around the valve with five array microphones capturing the sound propagation from the front, back, left, right, and top of the valve with a 0.5-meter radius. To determine the relationship between the acoustic power of the valve and its connection with structure-borne noise, four accelerometers were also placed on the valve surface geometry. They were used to characterize the surface velocity of the valve body with the flow-induced noise. Along with the primary sensors, other sensors were used to capture oil temperature and motor rpm. It should be noted that the oil temperature was not recorded during the experiments and was just monitored on a separate k type thermocouple display module; this ensured that during testing, the oil temperature did not deviate from the operating parameters.

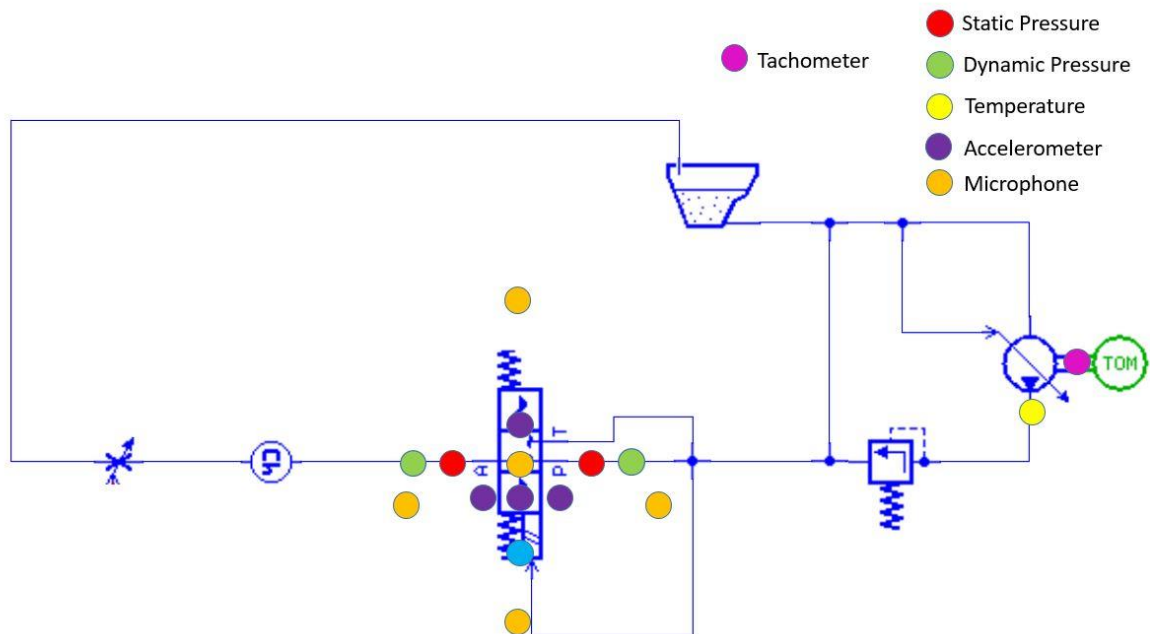


Figure 2-2: Sensor locations for accessory valve hydraulic circuit.

2.5 Sound Enclosure

It was determined early on in the project that the sound radiation of the electric motor would negatively affect the measurements taken when characterizing the valve acoustic noise. To remedy this, an acoustic enclosure was built around the electric motor to remove much of the acoustic energy from the lab. This enclosure was constructed out of wood studs and gypsum board, and because of the space limitations of the lab space, the free-standing enclosure is acoustically small compared to the wavelength generated by the motor.

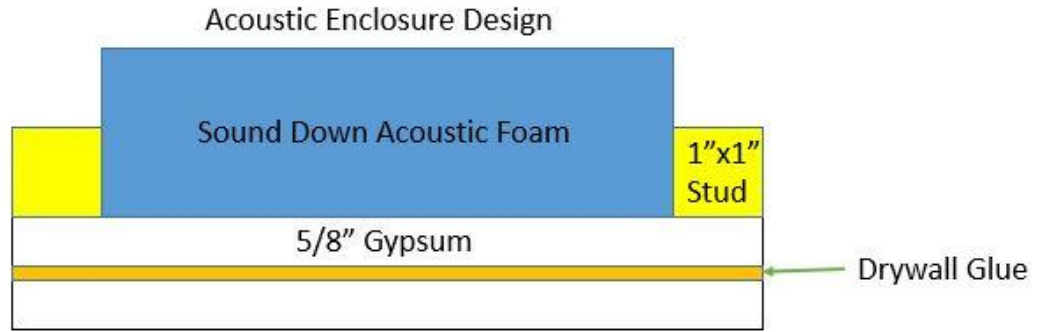


Figure 2-3: The acoustic enclosure design

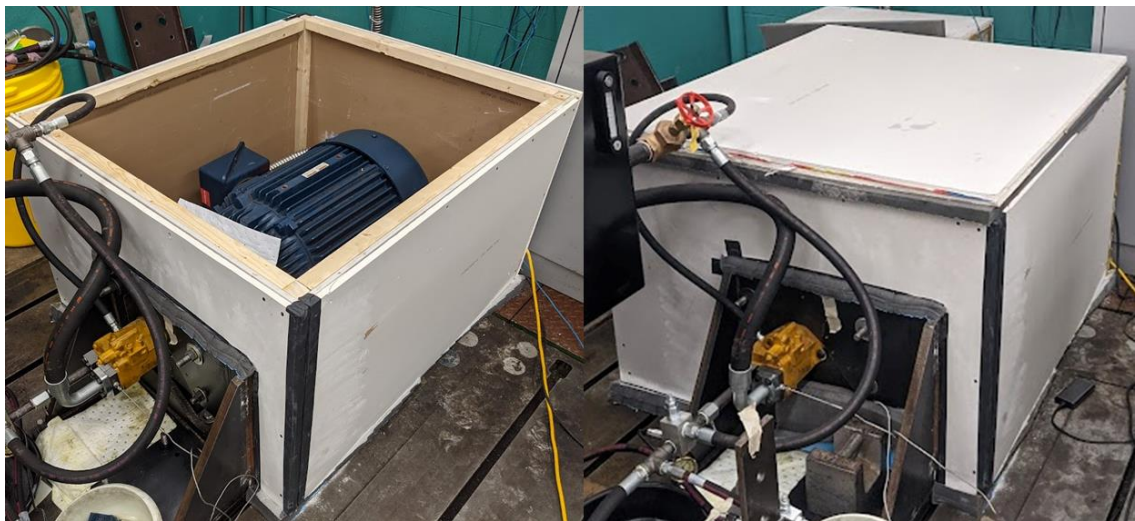


Figure 2-4: Acoustic sound enclosure for the electric motor. Closed-cell Soundown foam cladded the interior.

To determine the impact, the acoustic enclosure had on operating acoustic levels, a comparison method was used to calculate the noise reduction in the lab.

In figure 2-5, the known source, a blower fan, was placed near the unknown source, the electric motor, and moving averages of the sound pressure were measured using a sound level meter. The test was a 30-second moving average, with the SLM starting at 6 feet away from the source and then slowly moved away until it was 20 feet from the source. The 20-foot position was reached with 10 seconds remaining in the test, where the SLM was held until the entire 30-second run was complete. The room's absorption coefficient could be calculated from this initial SLM data of the known source. The variable L_w would be a 1/3rd octave sound pressure measurement, and L_p was the sound power of the known source provided from the blower motor literature. The last two variables are Q_θ which is the propagation field constant, and S which is the room's surface area. The final room absorption can be calculated with all of these values measured.

$$L_w = L_p - 10 \log_{10} \left(\frac{Q_\theta}{4\pi R^2} + \frac{4}{\bar{a}S} \right) \quad (2)$$

Once the known and unknown source testing was complete, the acoustic enclosure was installed around the motor, and the same roving SLM measurement was completed. The motor was run at 1000 rpm for both the pre and post- enclosure tests to provide stable acoustic signatures. With all of the room properties calculated, sound power can be calculated using the equation for the unknown source.

$$L_{pu} - L_{pk} = L_{wu} - L_{wk} \quad (3)$$

On the left-hand side of the equation, the variables L_{pu} and L_{pk} are the unknown and known sound pressure levels, respectively, with the right hand being unknown and known sound power levels. From this relation, the sound power of the electric motor can be estimated before and after the acoustic enclosure was installed. In figure 2-6, the sound enclosures impact on ambient acoustic levels is compared to baseline data.

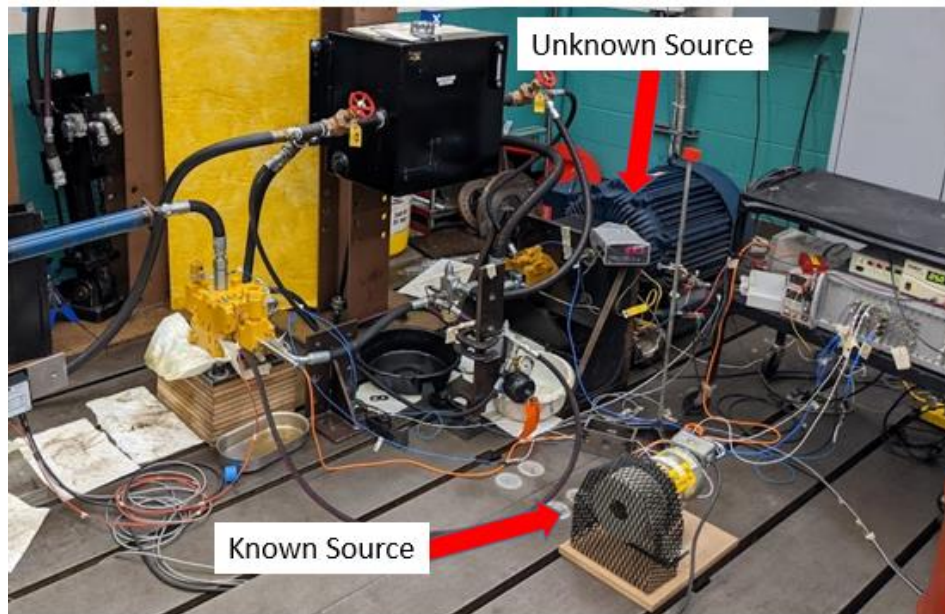


Figure 2-5: The known and unknown sources are shown in position for the test.

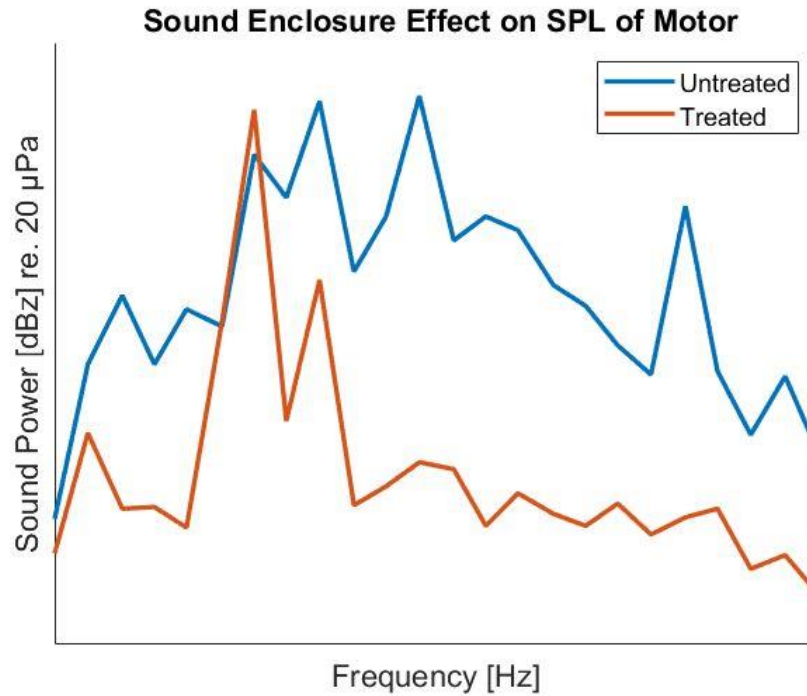


Figure 2-6: Sound enclosure noise reduction.

There was a reduction in Sound power across the frequency band after the sound enclosure was sealed. However, the sound level was not reduced at one of the octave bands because of the pump harmonics. Furthermore, the pump was not sealed within the sound enclosure which explains the lack of reduction in that octave band.

2.6 Brake Valve Circuit

The test bench had to be completely redesigned to accommodate the new circuit layout for the hydraulic brake valve. The control variables were also changed to

characterize the new system requirements properly. During the brake valve testing, the electric motor would not have to be running, and the accumulators instead supplied pressure. The oil temperature requirements did remain the same between the two test benches with the motor running at 1000 rpm until it reached 50 ° C. After the oil was up to operating temperature, the pump would continue to run as the brake pedal was actuated to flow the hot oil through all system lines.

The system kept the same motor, pump, and pressure relief valve, but now the circuit would pump the fluid through a hydraulic filter. Next, the fluid would move through a one-way check valve to hold the pressure at the accumulators to a preset operating pressure. The circuit was designed to have two accumulators independently supplying oil to the brake valves' top and bottom inlet ports. Once the flow entered the valve, it moved through either the top and bottom outlet ports, or it flowed directly back to the tank when the valve has finished its brake procedure. The fluid that moved through the valve outlet would proceed through an inline orifice and then actuate the slack adjusters. The slack adjusters were designed to mimic the brake response on the machine and provide flow resistance to the system. After this, the flow would move back to the brake valve, return to the tank line, and flow back to the hydraulic oil reservoir. This layout can be seen illustrated in figure 2-7 and accurately replicates the on-machine circuit behavior.

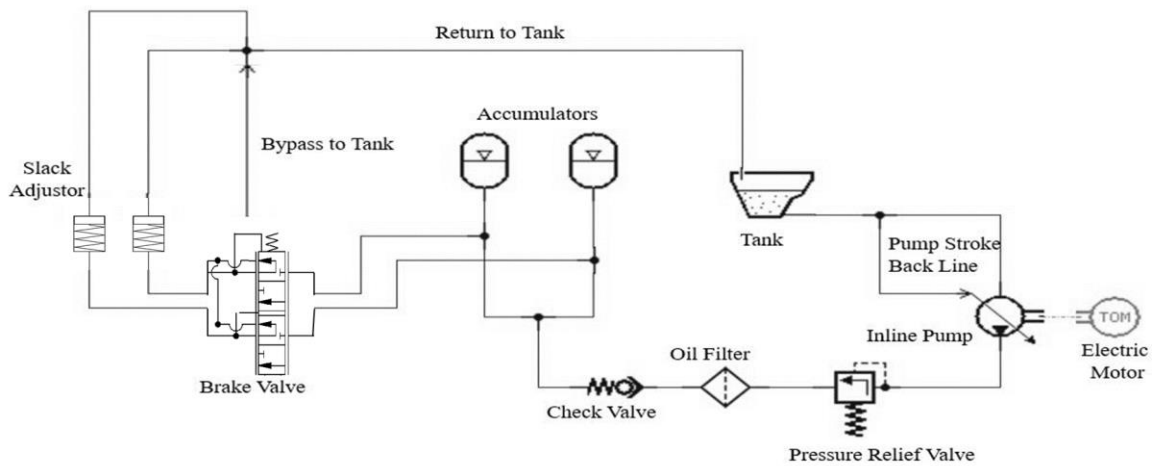


Figure 2-7: Brake Valve circuit major components and layout.

2.6.1 Fixture Design

Three different fixtures were designed and built for the hydraulic circuit to accommodate the new components needed for the test bench. The fixture requirements were that all components needed to remain in the orientation found on the machine and not introduce any outside variation to the measurements. To mount all components, a platform for the brake valve needed to be built along with mounting brackets for the slack adjusters and accumulators.

The first fixture built was a mounting bracket for the accumulators. On the machine, they hang vertically, so to ensure proper behavior, the orientation was kept the same. The vertical brackets were constructed out of $\frac{1}{4}$ " mild steel, which would not flex due to any hydraulic loading of the hoses. Before the

accumulators were mounted, they were charged with 680psi of pure nitrogen as per specification; the now charged accumulators were hung from the stand. Because dynamic pressure and acceleration were not intended to be measured at the accumulators, a modal test was not conducted to determine if the bracket's modal response was in the bandwidth response of the brake valve.

The main fixture was built to actuate the brake pedal assembly. This platform needed to support one operator and have low vibration levels to offer real-world boundary conditions for the valve. The bench frame was constructed of 1.5" square tubing with .120 walls and had a top plate of $\frac{1}{8}$ " mild steel. The platform measured 2'x4' to allow proper operator ergonomics and facilitate a repeatable actuation of the brake pedal. The hydraulic brake valve was the most instrumented component of the circuit. Several dynamic pressure and acceleration measurements were taken on the valve; the dynamic response of the platform was of great interest to ensure it did not interfere with the measurements taken on the valve. To address this, a rubber gasket was added between all metal-on-metal contact. To offer more isolation and support, a cross member was welded to the frame 14 inches back to the box in the area the brake pedal assembly was mounted. The breathing mode amplitude of the platform top plate was reduced and offered a stiffer mounting area for the brake valve. Lastly, a bracket was attached to the test bench to attach the string potentiometer (string pot) anchor. The string pot was bolted to the brake pedal with a small amount of cable out to preload the fixture and reduce any elastic deformation in the string

pot anchor fixture. With a stable sensor and anchor fixture, the sensor was then zeroed in the Testlab Software.



Figure 2-8: Brake valve platform. With string pot bracket.

The last fixture constructed was a bracket to mount the slack adjusters. This would orientate the slack adjusters vertically and allow the LVDT to operate correctly. Since the slack adjusters moved in unison, there was no worry they would interact with each other's dynamic response. This fixture was also constructed out of $\frac{1}{4}$ " mild steel, in order to reduce any vibration transferred by the flow moving through them to the displacement sensor. The construction and mounting orientation of the slack adjusters can be seen in figure 2-9.



Figure 2-9: Mounted slack adjusters (right) and the construction of the mount (left).

2.6.2 Brake Valve Test Plan

The first brake valve tested had internal geometry that created a characteristic “whooshing” noise as the valve spool is moved from fully closed to open. This valve is not currently used in machinery, but studying its characteristic sounds can assist in determining the geometric features that correlate with a poor noise profile and help design future spools, avoiding the undesirable geometry in critical locations.

Table 2.7: Whoosh valve test procedure.

Brake Valve Actuation Test			
Test Number	Total Run Duration [sec]	Brake Pedal Press Time [sec]	Brake Pedal Release Time [sec]
1	1	0.5	0.5
2	3	2	1
3	4	2	2
4	6	4	2
5	7	3.3	3
6	10	6	Hold
7	10	3	Hold

2.6.3 Brake Valve Control Variables

During the brake valve testing, pump harmonics were not present, thus allowing the data processing to go much easier when compared to the accessory drive valve. This simplification of the test procedure allowed only two independent variable to be tested: the brake spool position and inlet pressure. The actuation of the brake pedal using different press and release times allowed for a direct correlation to flow noise without much post processing. The brake actuation profiles seen in table 2.7 attempt to mimic the types of brake loads seen in real-world applications.

2.6.4 Brake Valve Dependent Variables

The sensors used for the brake valve testing focused more on the dynamic pressure and static pressure relationships in the fluid flow as opposed to acoustic and vibration measurements conducted on the first accessory valve. Focusing on the fluid flow through the valve inlets and outlets, a complete characterization of the flow properties was completed. Also, the new shift in focus required only one accelerometer and microphone to be used. Because of this change, the channel count was decreased from the accessory valve. These changes allowed more focus to be placed on the flow profile of the valve. Another change was the inclusion of temperature sensors into the frontend for this round of testing. It was believed that rapid compression and decompression of the fluid would change the properties of the hydraulic oil and impact the flow noise.

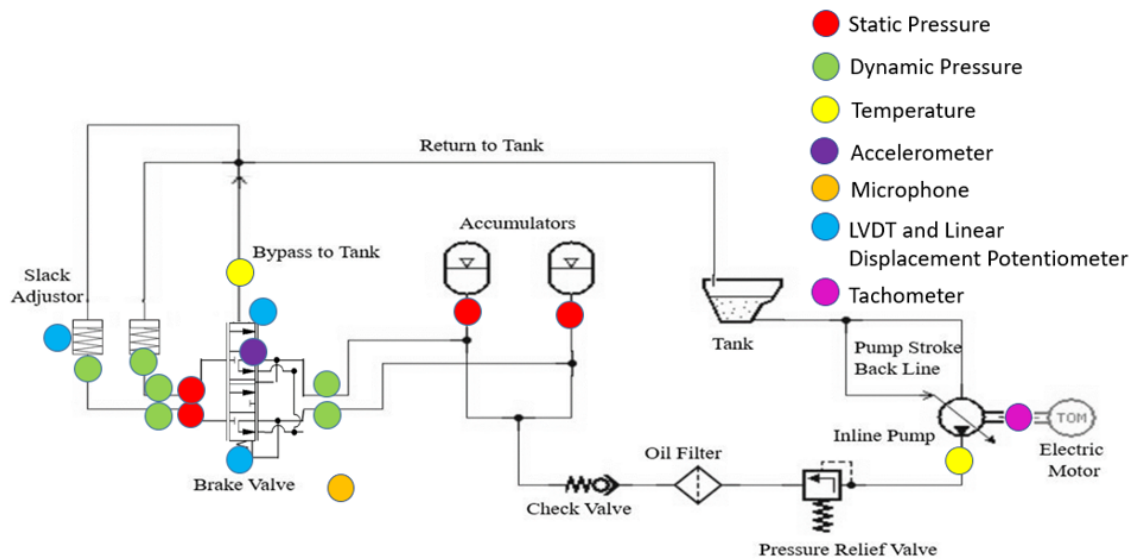


Figure 2-10: Brake Valve Sensor Location Diagram.

2.6.5 Fixture Modal Validation

A drive point modal test was conducted on the top plate to determine whether the rubber mats provided adequate damping to the brake valve structure. The tests were run twice, with one test having the platform unloaded and a second with an operator seated in the chair. Both tests showed that the system had adequate damping, and there weren't any significant platform modes excited in the bandwidth of interest for the brake valve. The test was conducted with one triaxial accelerometer glued to the bottom of the platform in between the two mounting locations of the brake pedal assembly. The structure was then excited in the vertical direction to excite the freest degree of freedom of the system. Ten averages were then taken for each test to calculate the H1 FRF of

the structure. This test concluded that the rubber matting offered enough damping to the structure, and it would not be excited by the dynamic valve response.

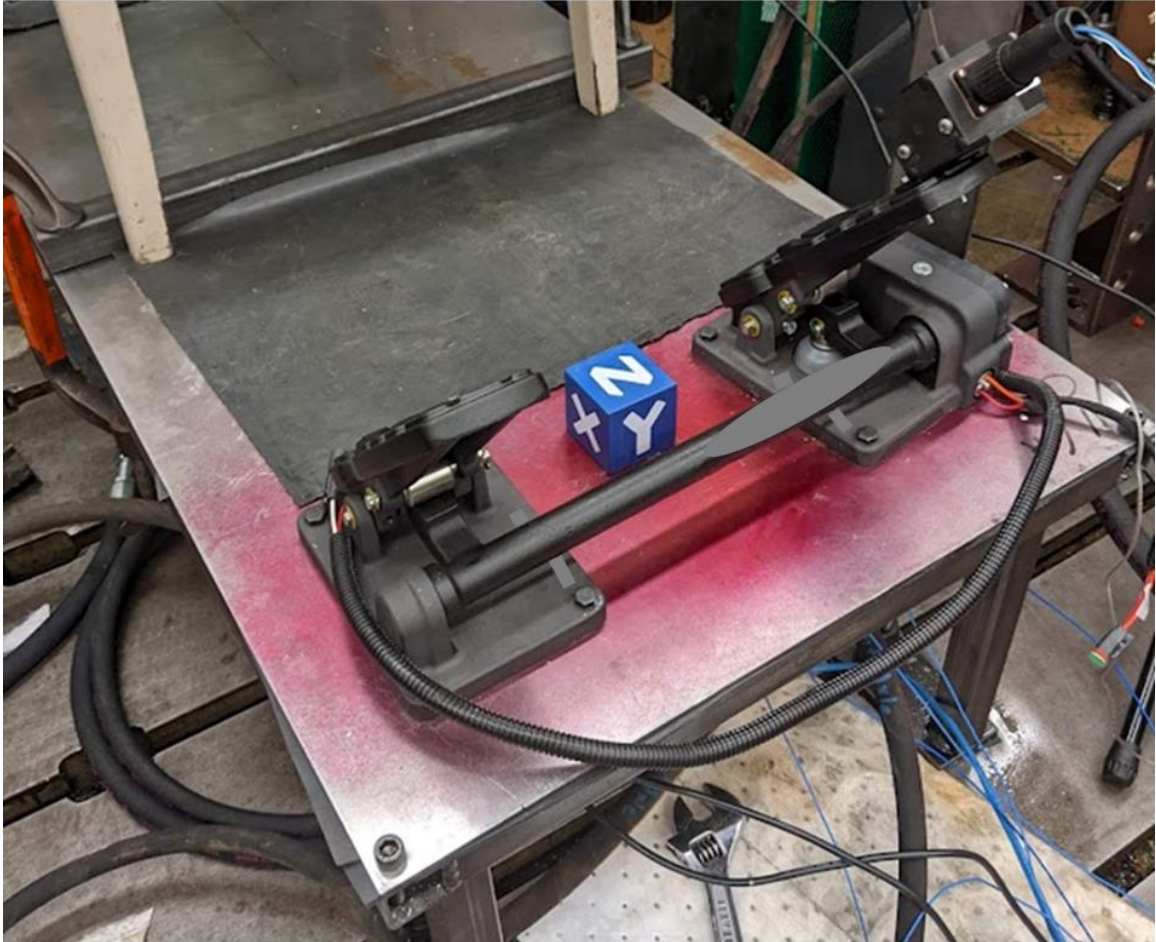


Figure 2-11: Coordinate cube representing accelerometer mounting location.

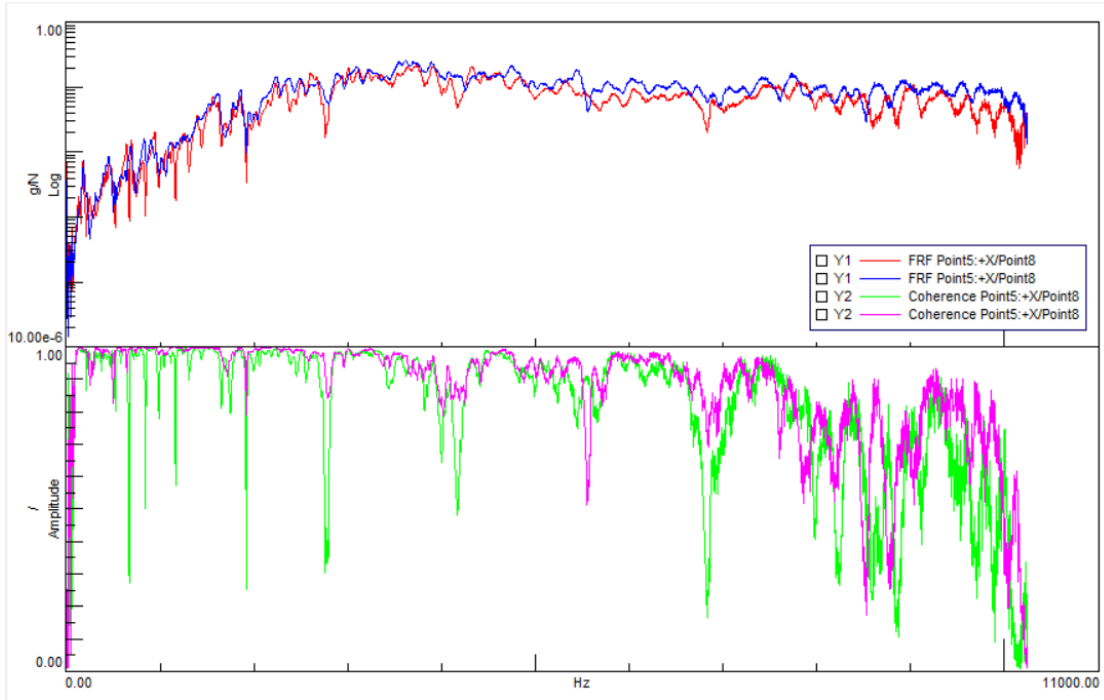


Figure 2-12: H1 FRF for valve frame excitation.

The top plot is the H1 FRF for the two runs recorded. And the lower plot is a coherence plot. Both tests showed no significant change between the test with an operator and without an operator. There is also a considerable confidence factor in the test seeing any dips in coherence correlate with anti-resonance of the structure.

3 Results

3.1 Accessory Valve Results

A lot of testing was conducted on the accessory valve, and many things were learned about the behavior. But due to the shifting scope of the project and unforeseen complications that arose late in the testing process, the project scope was moved on to focus attention on the brake circuit.

The most significant advance made on the accessory valve flow noise analysis was identifying the flow region. This region did not create a constant flow noise as the valve opened but would have two peaks of flow excitation. The first occurred when the valve first opened. This small open area would cause large pressure gradients inside the valve and cavitation. The second region for flow noise was as the valve opened to the max open area. This region was believed to be caused by the compensator closing and allowing the main valve to operate independently. These two regions were the most significant contributors to flow noise, with the noise decreasing dramatically after the flow matured and became stable. It can be seen in figure 3-2 the impact rpm has on the flow noise generation of the system. The increased rpm caused a more significant driving pressure on the valve's inlet side, which translates to increased pressure gradients inside the valve body. Overall the tests concluded that the most flow noise occurred at high RPMs meaning that there were higher inlet pressures and the largest pressure gradient across the valve. The final discovery was the

impact boundary conditions had on flow noise; initially, the two boundary conditions were used to determine if any fluid modes were created on the outlet side of the valve. However, there was no considerable flow noise change between the four-meter hose and expansion chamber.

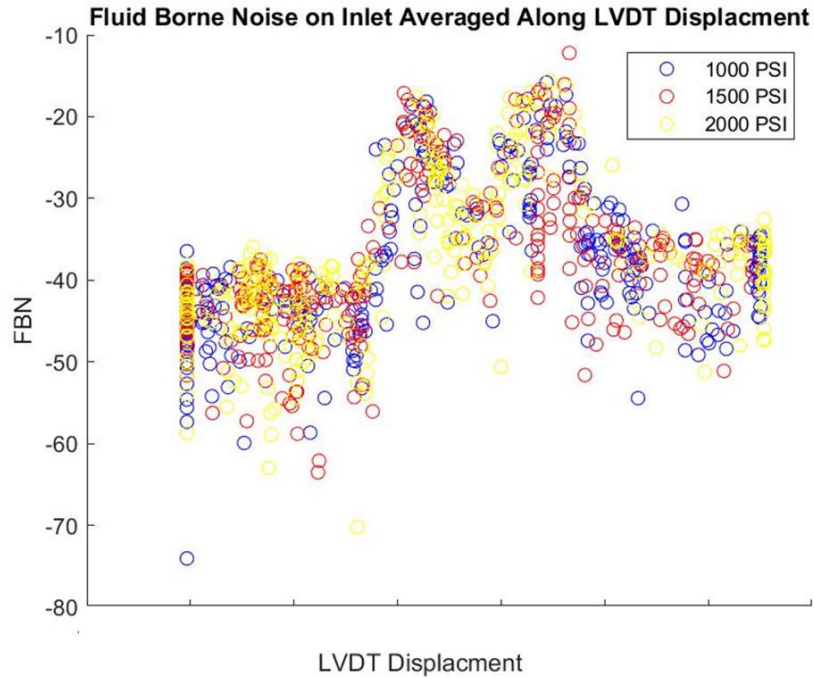


Figure 3-1: Accessory Valve fluid borne Noise at 1000 rpm

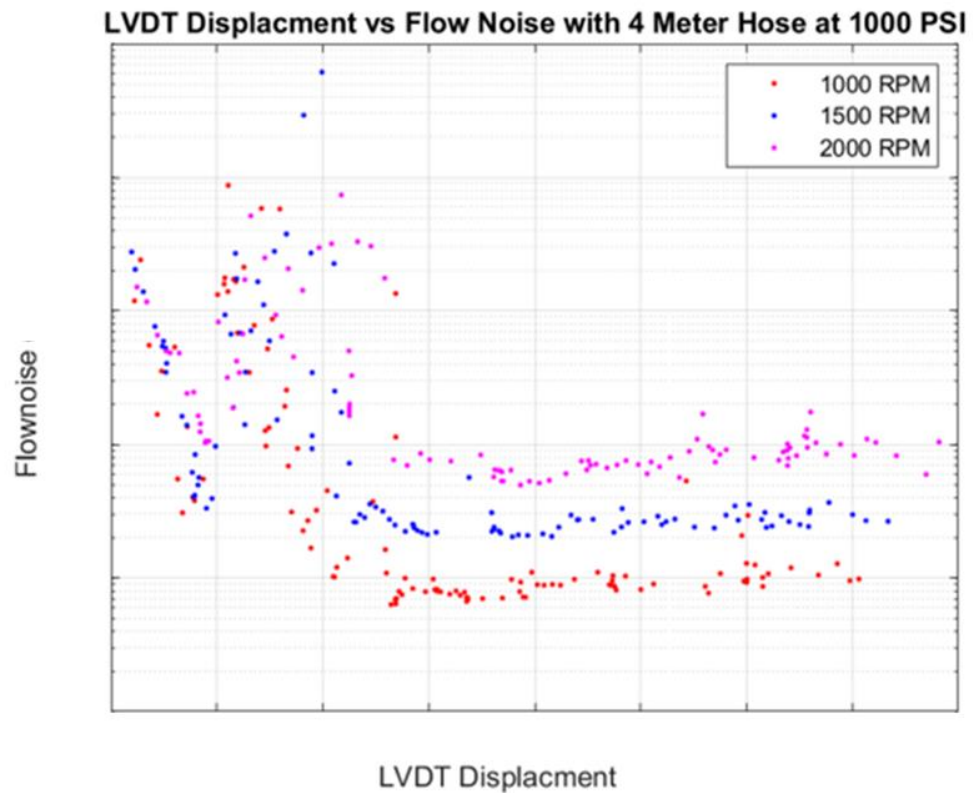


Figure 3-2: Drive Motor impact on Flow Noise.

During testing, it was found that shock events occurred during high rpm with low back pressure load cases. This new event had not happened before, so the data was reviewed to determine probable causes. As discussed previously, it was discovered that adaptations made to the valve to accommodate pressure measurement had actually introduced valve instabilities. A check valve spring had been removed to allow direct measurement of the compensator spool, which in turn was required to properly characterize the total open area of the valve with both the accessory spool and compensator spool. To prove this was the root

cause of the issue, the brake was tested with and without the check valve spring to determine if the overload events were linked to the spring. It was found that it was connected, and the spring would be required for correct valve behavior during testing.

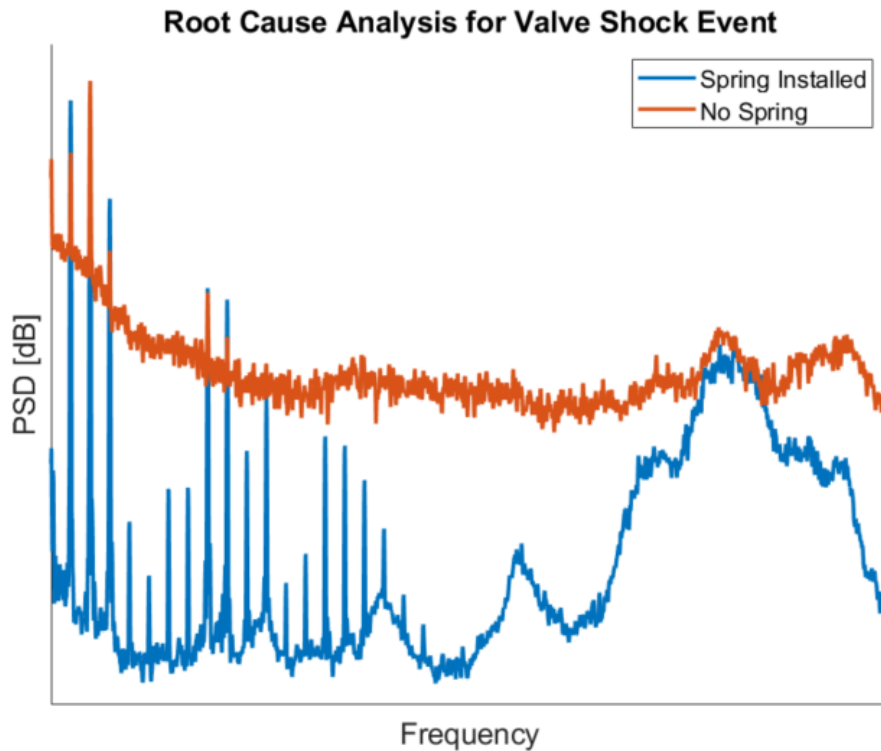


Figure 3-3: Accelerometer frequency spectra from valve body. The signal with the spring installed has much more harmonic data which is expected. However with the spring removed there is a large saturation of the sensor and useful data is lost.

Due to the evolving scope of the project and the new found difficulties surrounding the previously unknown complexity of the accessory valve, research of the accessory valve was stopped at this point. In the future, the data is still valid and could be used to estimate the flow noise of the valve during various flow regions. The method used to calculate flow noise had required the open area but seeing as this would have been impossible to predict with the valve functioning properly, a new approach would be necessary. The technique used during the brake valve testing does not rely on the valve open area, but instead will quantify the valve acoustic energy in relation to the position of the spool in the brake body. Next, the upstream pressure needed to actuate the valve is not being provided by a hydraulic pump but instead hydraulic accumulators. This would eliminate the need for the drive motor and pump to be running during tests. The pump had caused significant difficulty when removing harmonics from the flow noise without impacting the overall flow energy. With these changes, the project could be revisited in the future.

3.2 Brake Valve Results

The results of the experimentation for the whoosh brake valve were very insightful. The testing determined the acoustic energy created by hydraulic flow through the brake valve in seven distinct areas. The results are most effectively understood by breaking them down into four groups.

1. Valve Behavior in the Time Domain
2. Valve Behavior in the Frequency Domain.
3. Flow Behavior in relation to brake spool positions.
4. Energy Created in each distinct flow region.

After concluding the whoosh brake valve testing, it was chosen to use one run of data as a representative set to discuss all of the valve operations. While the overall energy created from the flow did change its response in the time domain to spool position followed a very clear and repeatable pattern. No matter the pedal press speed or inlet pressure the signal had the same features for all the runs.

Another key finding in the research was the identification of the flow regions of the valve and what geometric features in the valve body they correlated with. These findings are discussed in more detail in the sections Valve Flow Regions and Quantifying Flow Region Energy. Still, through the data processing, they were identified as the following seven regions. It was discovered that the valve spool did correlate with the movement of the brake pedal, but its response did have a small degree of independence and would react independently to supply constant pressure to the slack adjusters and not correlate directly with what was being input by the operator. For these reasons, all-valve responses and flow energy will be described with respect to valve spool position and not the brake pedal position.

Region 1: Initial spool resting position valve is closed

Region 2: Flow has entered valve inlet and pressure builds, but brake spool has not opened outlet port

Region 3: Flow occurs from the pressurized inlet to outlet and the brake spool reaches maximum displacement and begins to settle.

Region 4: No flow occurs, and the valve holds constant output pressure in modulating the position.

Region 5: The brake pedal is released, and the valve moves to a secondary modulating position as output pressure decreases.

Region 6: Brake spool drops from the secondary modulating position to its lowest displacement closing the valve.

Region 7: Brake spool resettles from the lowest displacement to the resting position

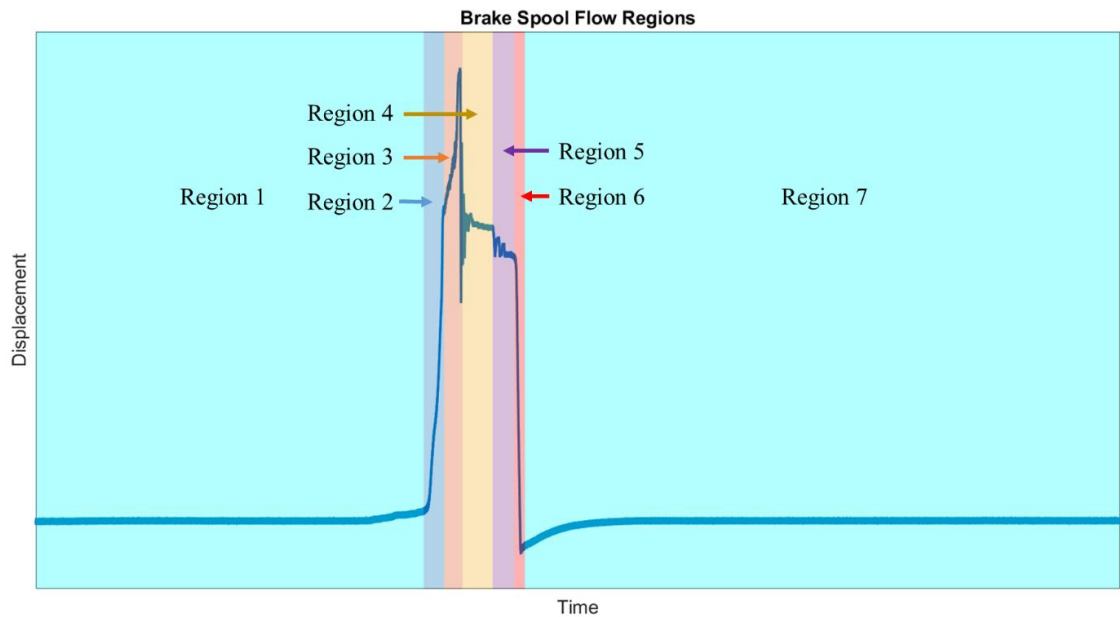


Figure 3-4: Valve flow regions are identified with the colored region.

3.2.1 Valve Sensors

The first set of plots was analyzed to determine how each measured parameter reacted when the valve was actuated. The uncertainty in how the system responds to brake pedal actuation is due to the internal design of the brake valve. The spool is not rigidly fixed to the pedal but is acted upon by the pedal through a series of springs. This dynamic input allows the valve to move independently in the valve body once it has been opened to regulate a constant output pressure.

To begin understanding how the system operates, the relationship between the slack adjuster, brake pedal, and brake spool must be understood as they move together to create a braking action on the test bench. It was found that

when the brake pedal is initially actuated, the spool moved in a very uniform fashion, but as the pedal reaches max displacement, the brake spool begins to move independently of the brake pedal, and instead, its position is controlled by the output pressure of the system instead of pedal position. Another key takeaway is the delayed response of the slack adjuster; it was found the delayed opening of the slack was due to flow not occurring until the 3rd spool region. This meant that the first part of the braking procedure did not apply any force to the slack adjusters.

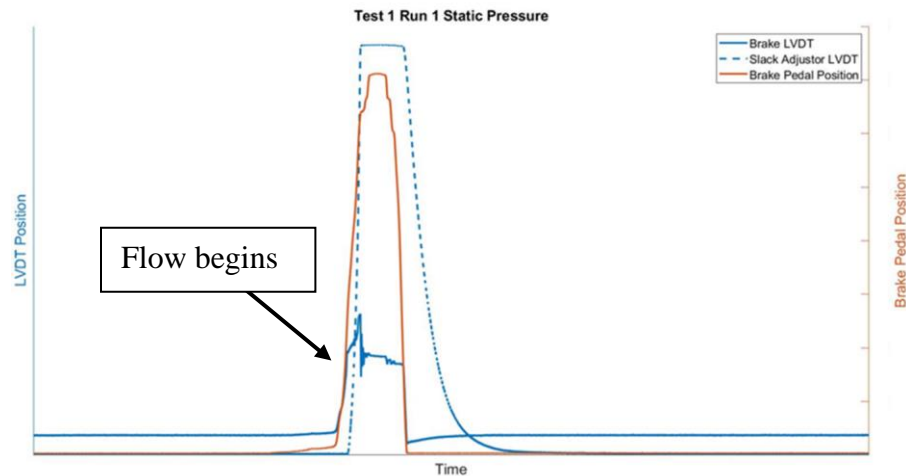


Figure 3-5: Overlay of all displacement measurements, showing the time dependent position relationship of components.

In initial discussions for instrumentation of the test bench, there was concern that temperature inside the valve body might vary, causing physical viscosity changes in the fluid. This change would ultimately impact the flow noise generation. During testing, this was not found; instead once the valve was

opened, the temperature dropped by only a few degrees Celsius. The drop in temperature is due to the system layout not being able to circulate hydraulic oil the same as on the machine. With the pump running, it was able to heat the oil up to operational temperatures within the reservoir and pump circuit, but as it moved to the valve and slack adjusters, it did not flow. Instead, it would flow from the accumulator to the valve, then fill the slack, and once the pedal was released, the oil would return to the valve and return to the tank line. This limitation of flow made the entire system problematic to reach full operating temperature and created the temperature drop seen in figure 3-6. The key takeaways are that temperature did not play any role in flow noise creation on this test bench. While some issues did arise at getting the system to operating temperature they were still within the operational parameters of the machine. New test benches could include a bypass circuit to move warmer oil to all the components if this needed to be investigated further.

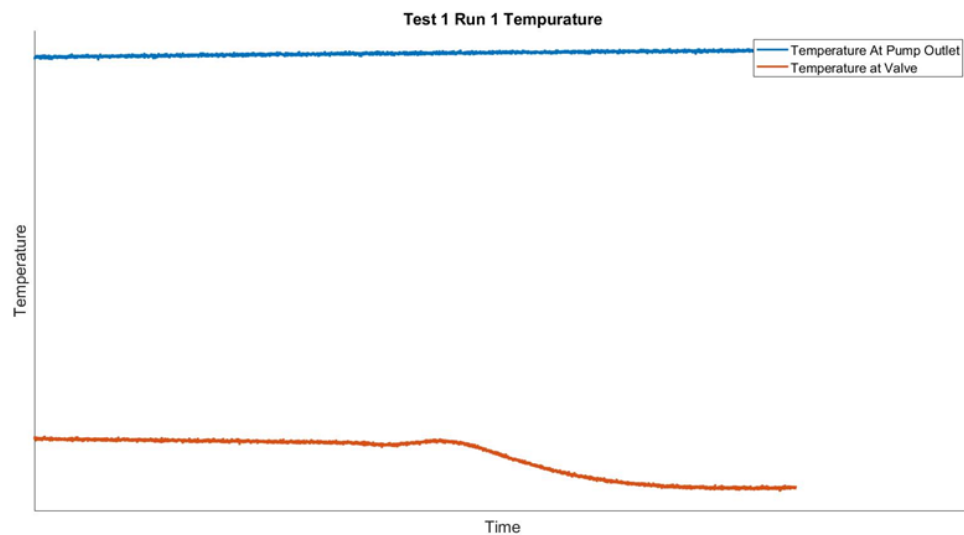


Figure 3-6: Operation temperature is taken for the system during valve operation.

The following analysis done was looking at the frequency and time response of the six dynamic pressure sensors. Four of which were on the inlets and outlets of the valve and two on the orifices downstream of the valve. It was essential to study each valves' ports to understand what was happening as the valve was opened. While it was understood that the valve created flow noise, it was unknown exactly when in the stroke or exactly what ports during the stroke were the most significant contributors to flow noise. Using the dynamic pressure sensors on each of the ports, it was determined that the outlet ports created more flow noise as seen with the larger excitation frequency range. A sample spectrogram can be seen in figure 3-7

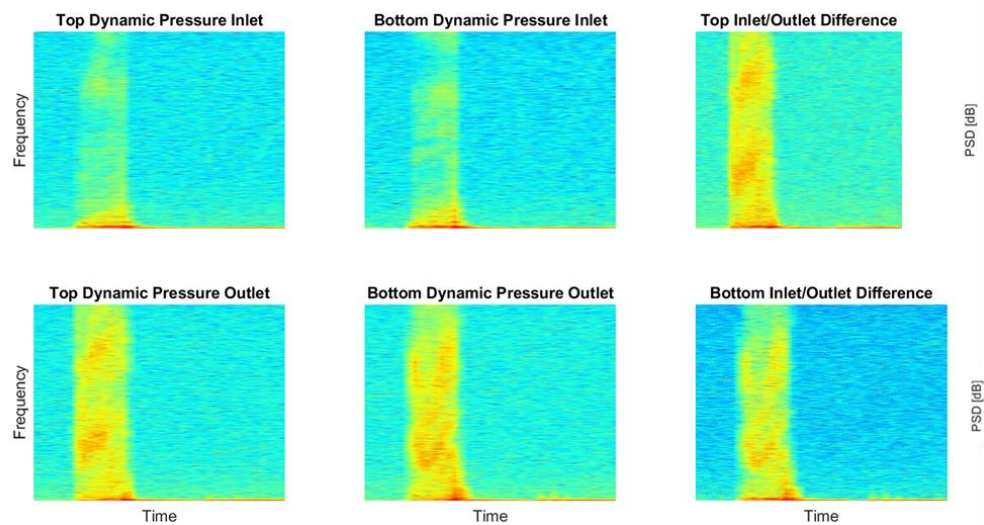


Figure 3-7: Spectrogram of valve opening. Most flow noise is limited to region 3 with increased dynamic pressure on outlet ports.

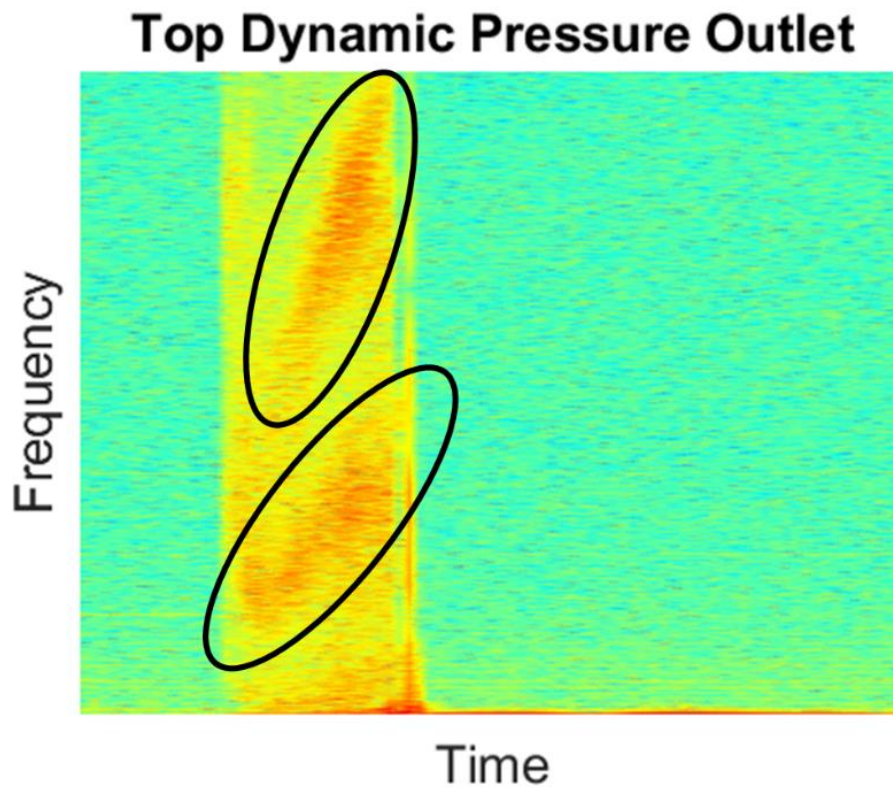


Figure 3-8: Valve Excitation regions

It was found that there were two main frequency areas excited by the flow through the outlet ports of the valve. They appear to be broadband excitations that increase in frequency as time passes and the flow stabilizes. It was determined that these excitation regions have higher energy when the valve is pressed slowly, such as tests 4 and 5. It can also be noted that the energy found in the dynamic pressure sensors was mainly focused in region 3. Once the flow has stopped, and the valve moves to region 4, where there is no flow, the spectrograms return to background noise levels as seen in figure 2-7

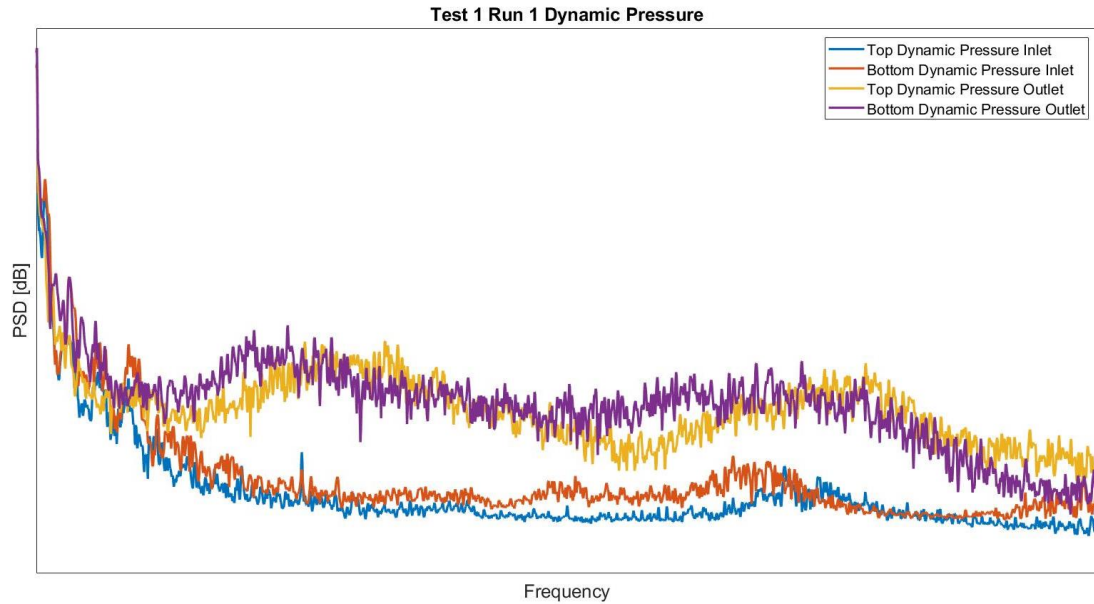
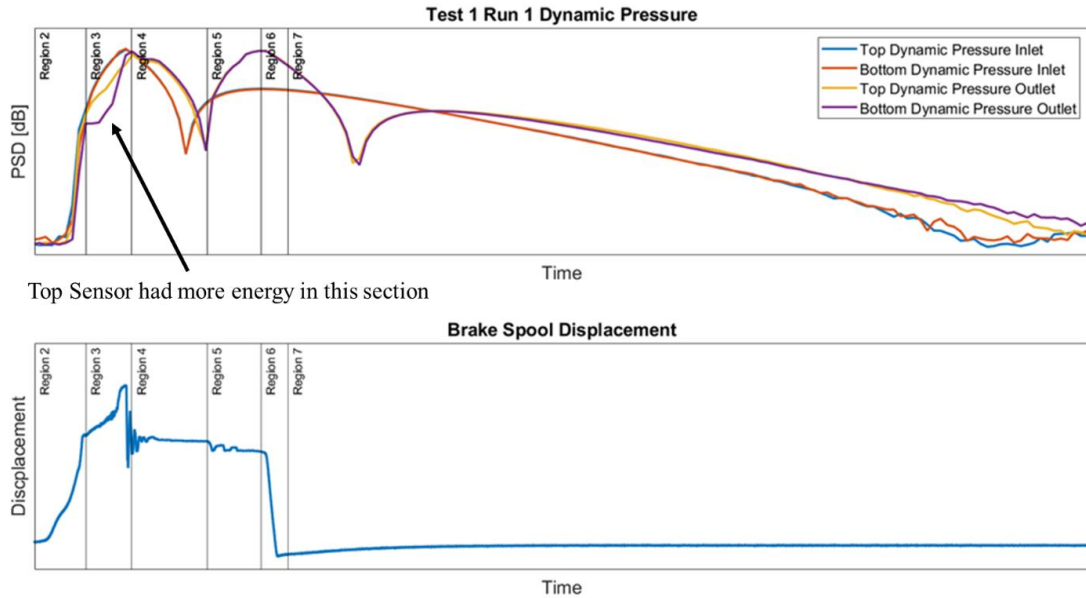


Figure 3-9: Frequency-based PSD looking at the energy response of the four-valve ports.

Cavitation noise is supposed to be a broadband excitation of energy across the entire frequency spectra. This plot was investigated to ensure there wasn't any harmonic data interfering with the flow noise measurements. Also, the difference in power between the inlet and outlet ports can be easily visualized. Another finding was that during rapid strokes of the brake pedal, such as tests 1 and 2, the top outlet port on the valve created substantially larger broadband excitation when compared to the bottom port. The energy disparity is not as severe when investigating tests with slower pedal sweeps of tests 4 and 5.



Top Sensor had more energy in this section

Figure 3-10: Time-based PSD for inlet and outlet ports correlated to brake spool displacement.

It was interesting to see a close correlation between the valves six dynamic pressure sensors and the brake spool LVDT. They both climb steadily until they enter region three, where the inlet energy is higher than the outlet energy. Also, the top outlet energy is more elevated in region three than the bottom outlet energy, which is consistent through all different test procedures. The drop in dynamic pressure was thought to be caused by the absence of flow when region 4 begins. In regions 5 and 7 where the sensors see a dramatic reduction in energy correlates when the pressure stabilizes through the valve.

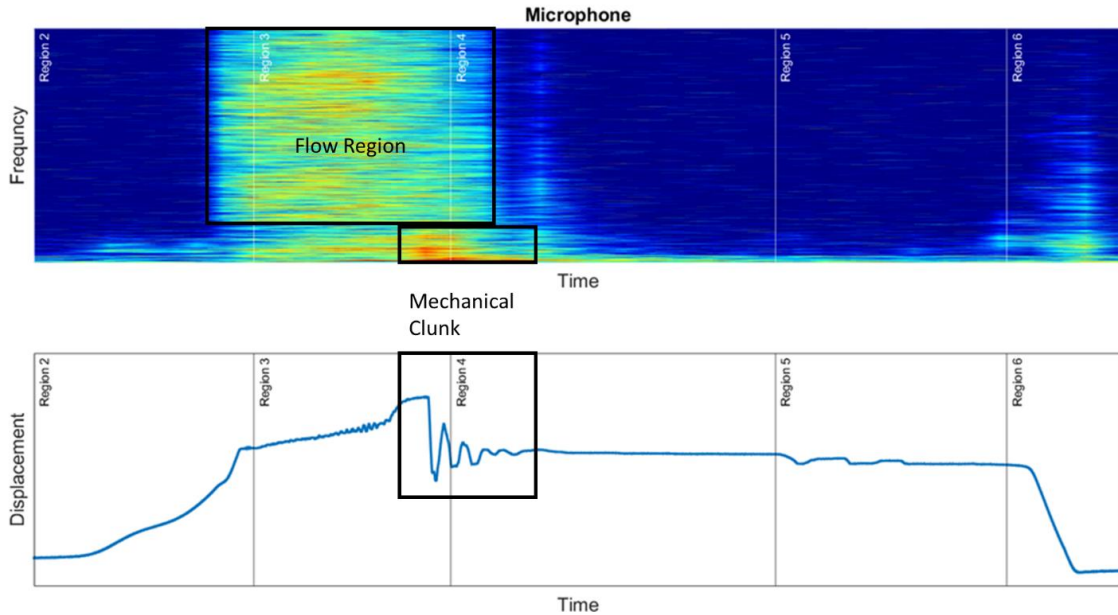


Figure 3-11: Acoustic Identification of mechanical clunk.

It was noted that a mechanical clunk could be heard under certain operating conditions when pressing the brake pedal. This was identified when processing the machine test data. This was of concern to determine under what conditions this anomaly was found and why it happened. This stabilization is more violent and causes more procurement clunk in tests 1 and 2, while by test 3, the clunk has substantially lost energy. By test 4, the clunk had dramatically lost energy.

3.2.2 Orifice Sensors

Downstream of the valve, an orifice was placed in each line before the slack adjusters to mimic the on-machine design. In real-world applications, the orifices are used to reduce noise as the flow from the valve enters the wet brakes in the

axle. They were necessary to ensure the test bench operated as close as possible to the actual circuit. During the analysis of these orifices, it was found that the left orifice had more energy and also more broadband excitation when compared to the right orifice. It is also important to note that the left orifice is in line with the top outlet, and the right orifice is in line with the bottom outlet. When the valve is opened rapidly, it is observed that more flow noise is created by the top outlet when compared to the bottom valve. It was also noted that when the valve is opened slower, as seen in tests 3-5, the broadband difference between the left and right orifice was eliminated.

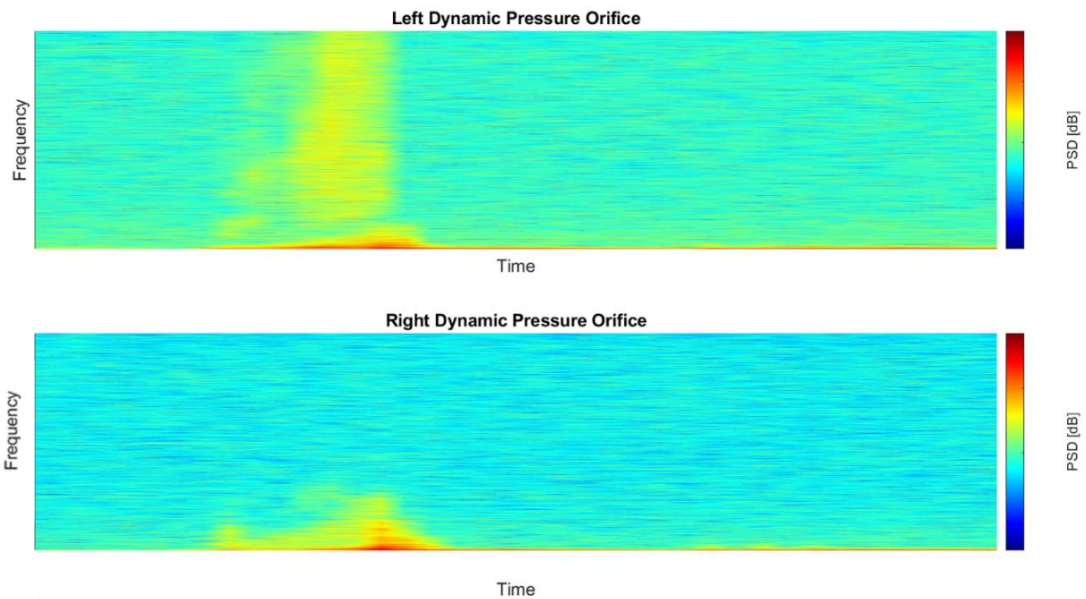


Figure 3-12: Comparison of Broadband dynamic pressure between orifices.

The following finding was the narrowband excitation found in all PSD and spectrograms recorded from the orifices. This is believed to be a small whistle created in the fluid as it flows. Overall, this was not impactful on the flow noise calculations and was also inaudible, so it was not investigated further to identify its relationship with the valve. It was also interesting to see that the frequency of the left orifice whistle was precisely twice as much as the right orifice. Another interesting finding was that the right orifice had much higher amplitude low-frequency energy and also had a more response in the high-frequency region.

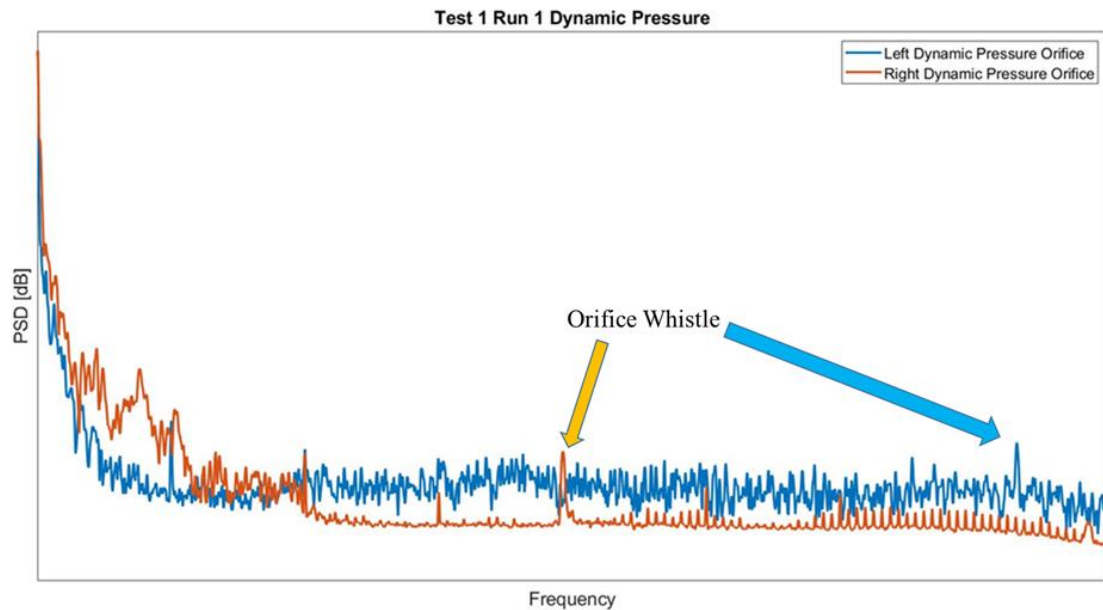


Figure 3-13: Orifice PSD in the time domain. The possible whistle narrowband responses have been identified.

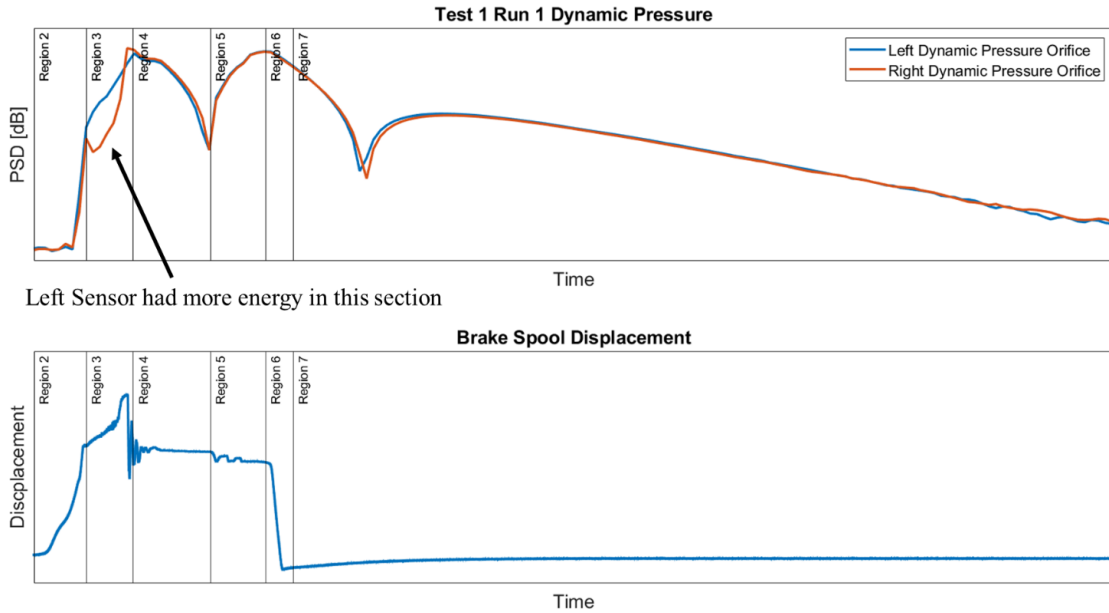


Figure 3-14: Orifice PSD in the time domain. They mirror the dynamic pressure signals on the outlet ports of the valve.

The main finding from the time-based PSD is that they perfectly mirror the outlet port signals. There was little to no distortion to the pressure ripple as it moved through the hose. Also, the pressure drops seen when pressure is released from the circuit correspond to the beginning of region 5. This pressure drop occurs when the operator begins lifting their foot off the brake pedal and closing the valve. The energy difference in the left and right orifice PSD can also be seen in the time signal within region 3. This difference was documented in all runs; no matter how fast the pedal sweep occurred. It should be concluded that the top outlet produces more broadband energy and has more energy in region three. In comparison, the bottom outlet produces less energy in region three and does so

at lower frequencies. All tests corroborated this conclusion with the most significant difference in the fast pedal motions.

3.2.3 Valve Flow Regions

When analyzing the flow characteristics of the valve, it was determined that because the spool was equally acted upon by the pedal input, flow pressure, and modulating pressure, all-region distinctions would be developed and relate to what the spool displacement was doing when flow occurred. This correlation between valve flow and spool position produced the seven regions introduced before. Of the six indices used for each run, four correlate to the flow of fluid through the valve. As seen in figure 3-14, four indices are shown, with the first being when region 3 starts and flow moves through the valve and begins filling the slack adjusters. The second is when region four starts and the flow stops with the brake spool moving into the modulating position. The third indices shown is where region 5 begins, and the operator releases pressure from the foot pedal, and the pressure built up in the slack adjusters flows back to the valve and the return to tank line. The last Indices are calculated by adding the slack adjuster return time to the third indices; this allows slack to be back to its initial position.

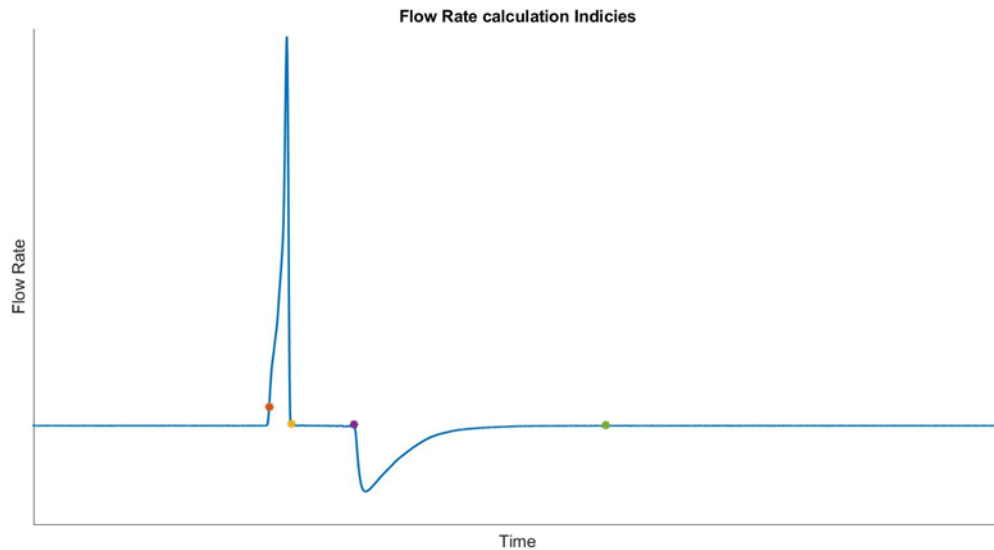


Figure 3-15: The four indices described are plotted on a flowrate plot.

With the flow indices identified, the next step was to validate the calculations done to determine the valve's flow rate and the volume of fluid that flowed during the pedal actuation. The flow through the valve would have been difficult to calculate. The slack adjustor was used to determine the valve flow rate. This was calculated using the following equation.

$$\textit{Flow Rate} = \textit{Slack Piston Velocity} * \textit{Piston area}$$

To validate the indices chosen when calculating the energy in each region, the flow volumes were calculated by taking the area under each curve and summing the difference. It was found that this method of determining the valve flow was very accurate and would return values with at most .05 ml of difference of flow

into the slack adjusters and flow back to the valve. Figure 3-15 it is shown how the slack adjustor displacement was used to calculate the flow rate.

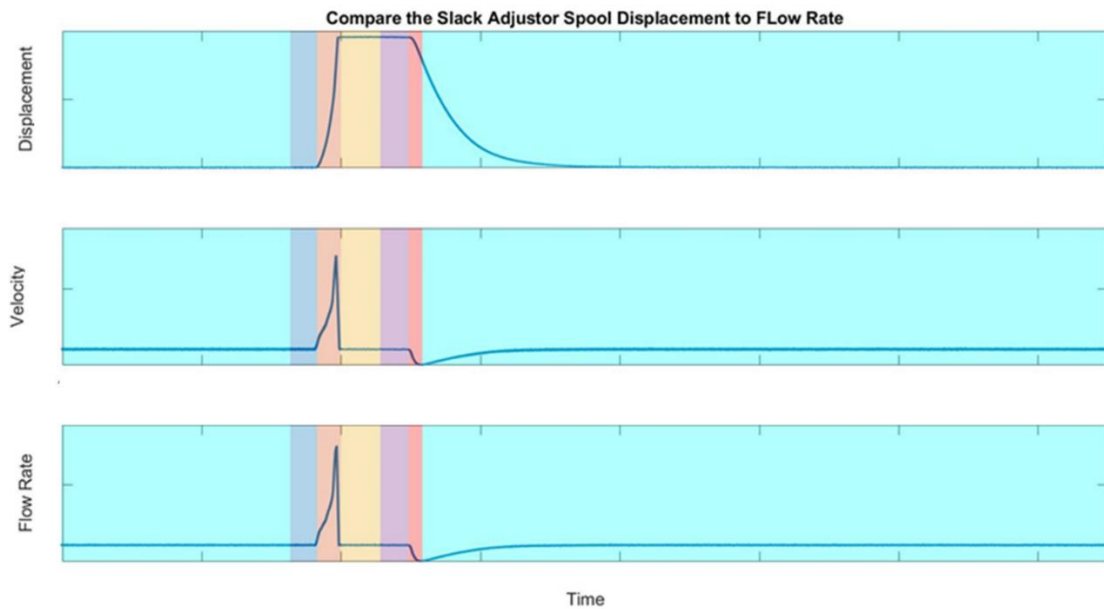


Figure 3-16: Flow regions overlaid with flow rate derivation.

A key aspect to further understand the brake valves behavior is to investigate how the valve parameters interact with each other throughout each of the flow regions. The following plots are displaying key areas one parameter was seen impacting another. This interaction was never documented before and understanding how these parameters affect each other will allow further engineering to isolate the areas that cause undesirable flow responses and mitigate them using adaptive integral geometry.

The first plot seen in figure 3-16 shows the relationship between flowrate and the brake spool position, this relationship has two key regions, with the first

being region 3. This area is where all the flow moves from the valve to the slack adjuster, it is characterized in the brake spool data as the first hitch of the curve to the first drop in position after the LVDT signal peaks. This region is where most of the noise is created and has been determined to be caused by the valve cracking open as seen in figure 3-19. The second region of interest is region six where the brake spool drops from its second modulating position to its lowest displacement. In this region, the fluid returns from the slack adjuster to the valve.

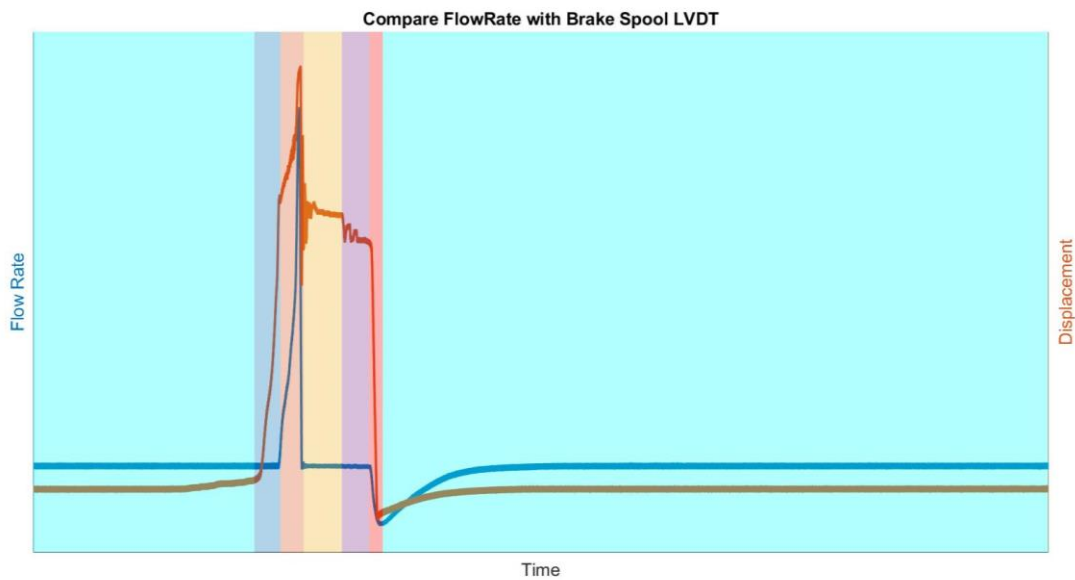


Figure 3-17: Correlation of flow rate to the region of the brake spool.

Next, it was interesting to see the relationship between the brake pedal and the static pressure sensors. It was shown that as the flow initiated in region 3 the pressure also began to drop in the accumulators shown as the black curve in figure 3-17 this drop stopped once the valve began modulating flow in region

four. Also in region four, it is seen that the brake pedal reaches maximum displacement at the same time as the static outlet pressure. This relationship shows that after the valve has been opened and flow has stopped after region 3 the pedal input directly correlates to the outlet pressure of the system. When the pedal is decompressed the static pressure immediately drops and by the time the 6th flow region the pressure is back to its resting position and the spool and slack adjuster return to their final position.

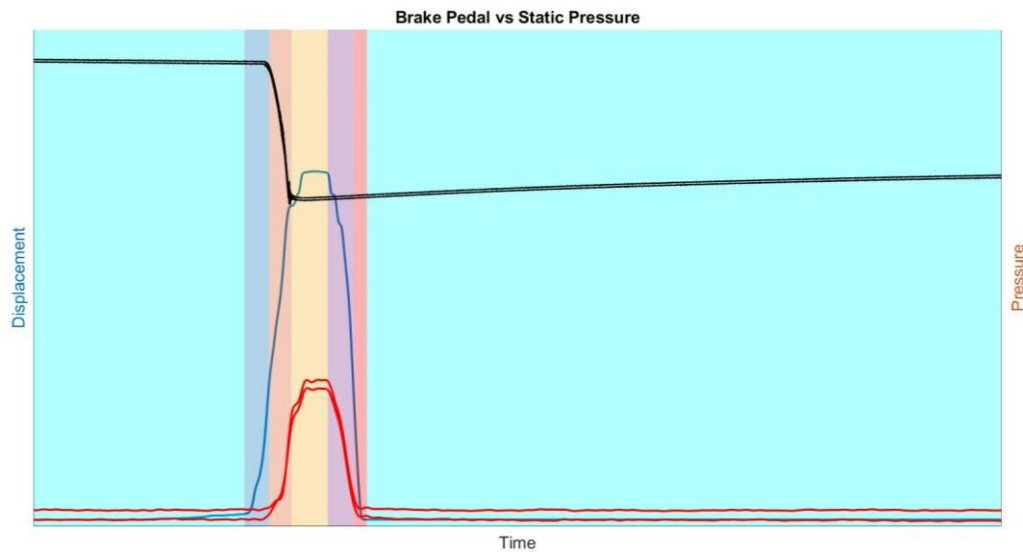


Figure 3-18: The black curve is the accumulator static pressure supplying oil to the valve with the red curves being the static outlet pressure of the valve.

The last variable correlated to flow rate was the acoustic energy measured by the microphone off of the valve. It was discovered that region 3 had the most noise generated with acoustic energy starting in region 2. It was found that region

2 opened the inlet of the valve and started allowing fluid to build pressure inside the valve body. The valve then opens in region 3 which produces the acoustic noise from the valve. This finding was very important to the project the exact location of the spool was able to be determined where this high acoustic energy was created. Another interesting finding was the peak acoustic noise correlated with the maximum flow rate through the valve. Proving again that the flow noise created during a braking cycle was isolated to one very specific region in the motion of the valve. A second smaller excitation can be seen in region 6 as the flow moves back through the valve, but this region does not have enough energy to be detrimental to the operator's experience when driving the machine. It is for that reason the investigation to flow noise was focused on region 3.

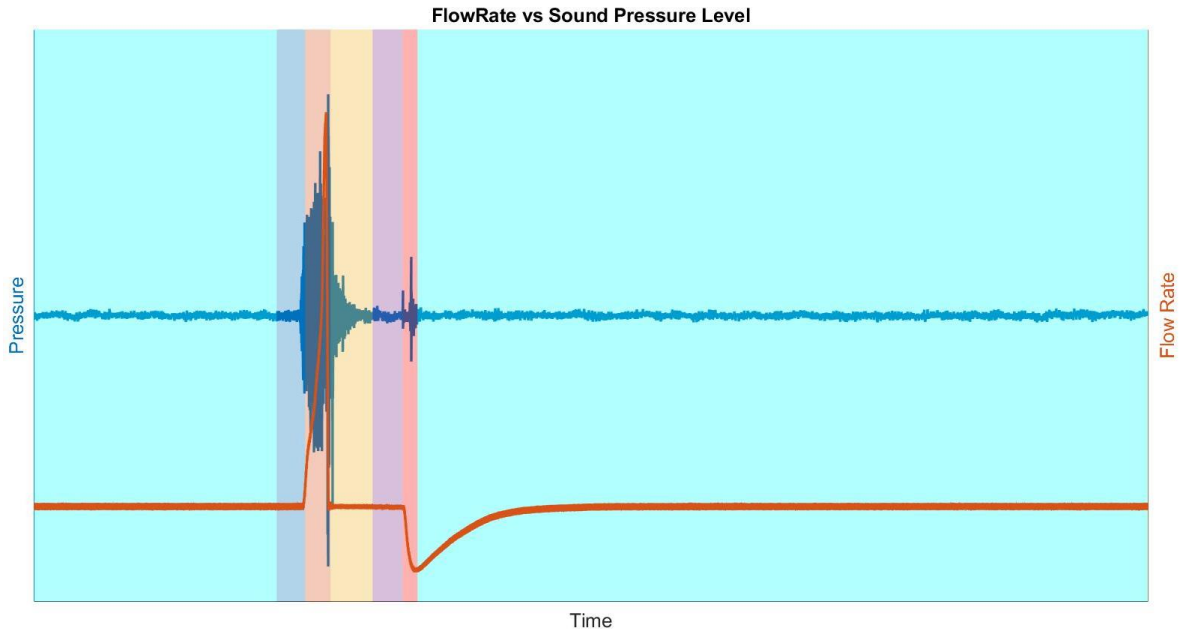


Figure 3-19: Acoustic energy compared to the flow rate of the valve.

3.2.4 Quantifying Flow Region Energy

The final set of analyses done was quantifying the total energy in each region for all of the tests conducted. It was determined that using a vector norm would be the easiest way to identify the variance of power in each run. Using this method, the dynamic signals from the dynamic pressure sensors, accelerometer, and microphone were used to determine how the overall power changed in each region as the spool was actuated. In figure 3-19 the top dynamic pressure sensor was evaluated with a comparison between the inlet port and outlet port. It was discovered that region 3 had the most energy in the inlet port but region five had the most energy in the outlet port. Seeing as most acoustic energy is created in region three it is believed that the inlet port contributes more low frequency energy when compared to the outlet ports which have a broadband response. This stance is further supported with the observation of none or very little acoustic noise in regions 4-6 where the outlet power is the highest. The bottom and top ports also showed very similar behavior across all runs but region 3 did seem to have more energy in the top outlet when compared to the bottom outlet. These findings supported the observations made in the spectrograms and time based PSD's.

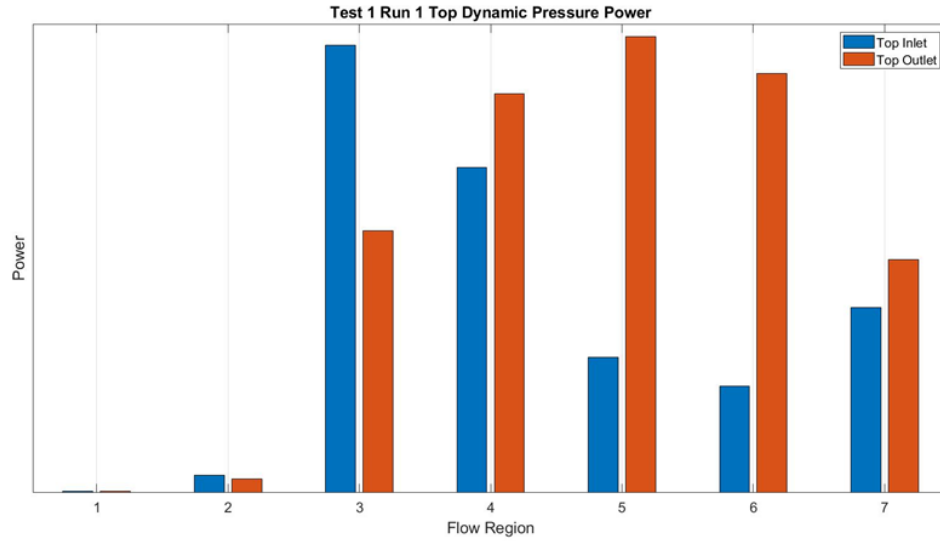


Figure 3-20: Top dynamic pressure sensor power comparison for inlet and outlet valve ports.

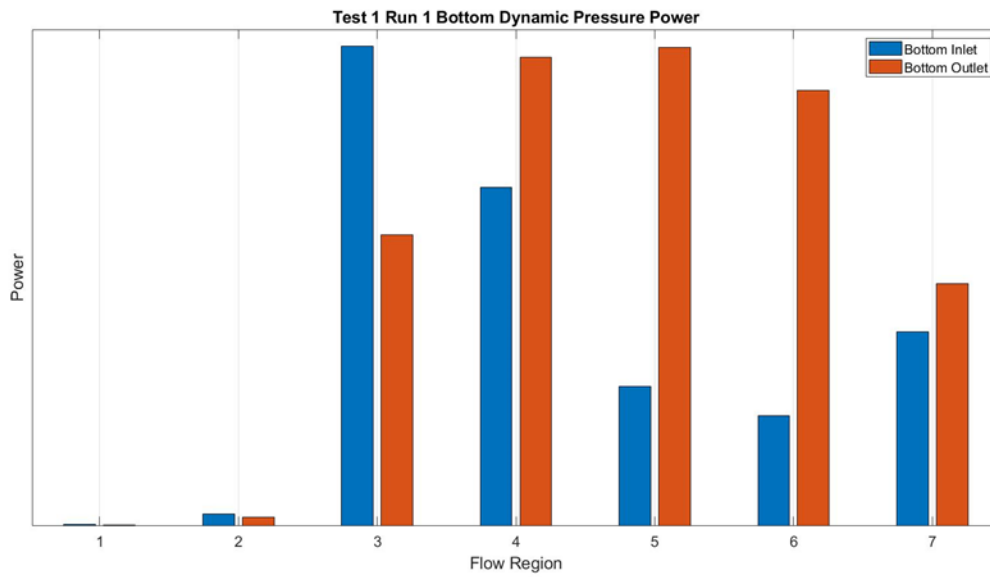


Figure 3-21: Bottom dynamic pressure sensor power comparison for inlet and outlet valve ports.

The next sensor analyzed using this method was the accelerometer data. The orientation of the accelerometer was with the Z axis parallel to the brake spool movement with the X and Y creating the normal plane. Overall this data showed much of the same results as all the other methods of analysis. It was expected the accelerometer would have the most vibration in region three along the Z axis. So this finding was used to just support all of the other conclusions made.

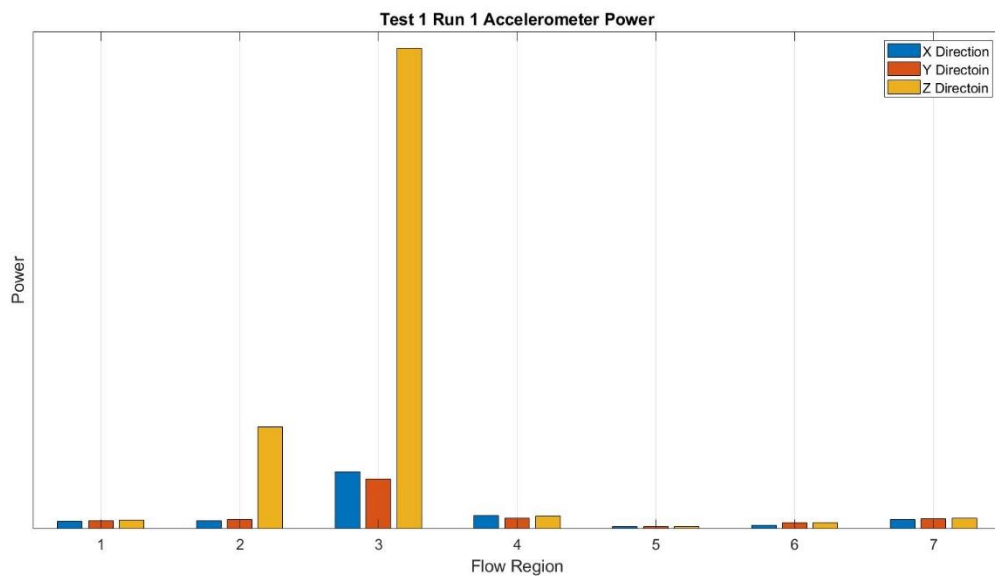


Figure 3-22: Accelerometer Power measured in three-axis for each flow region.

The final data analyzed with this method was the microphone data however, instead of doing the $(2norm)^2$ method the sound exposure level was

calculated. This method was used to more accurately represent the sound experienced by the operator. This formula not only accounts for the perceived loudness of the sound but also the total duration of the sound generated. Using this formula, it accounts for both the intensity of the exposure and duration. So even though region three had far more energy it was very short in duration meaning the total impact on sound exposure level was not as great, the formulation for sound exposure level or SEL is shown in.

$$SEL = Leq + \text{Log}_{10}(T) \quad (4)$$

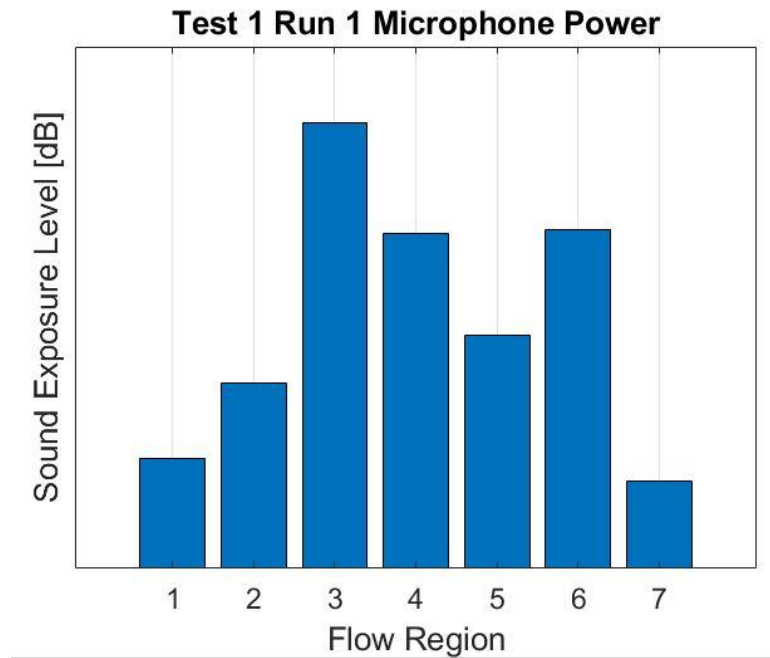


Figure 3-23: Microphone SEL during fast pedal sweep.

3.2.5 Dynamic Parameter Evolution Through Testing

The last technique used to characterize the flow noise through the brake valve was taking all of the bar chart data and creating a matrix with the data. Then the matrix was normalized using the highest value in each plot as the reference dB. Using this method, it is quickly discernable how the energy in each flow region changed over the course of all the runs. It was found that more energy was created when running the test at higher pressure. Then with each subsequent run, the static pressure in the accumulators would be lower than the previous test. This trend is most prevalent in figure 3-24, which depicts the microphone data. As discussed, region 3 created the most acoustic energy when the test was conducted for each of the first runs when the accumulators were full. Because the first run has the largest pressure on the inlet of the valve. it was expected that flow noise would be the highest for the first runs of each test case. The most surprising finding was that the second test case produced slightly higher noise levels than the first test, meaning a longer pedal sweep actually produced more noise. Next, it was found that the second-highest energy was the fourth test, with both tests two and four designed to have longer sweeps than their counterparts it was interesting to discover they produced more acoustic energy than all the other tests.

	Microphone Normalized Sound Pressure Level dB						
Test 5 Run 3	-11.8	-18.4	-2.1	-11.8	-22.3	-25.9	-14.4
Test 5 Run 2	-13.8	-17.6	-1.0	-12.0	-20.8	-25.4	-11.8
Test 5 Run 1	-13.2	-14.5	-1.0	-12.7	-20.7	-27.2	-14.0
Test 4 Run 3	-15.0	-17.2	-3.0	-12.3	-21.6	-24.8	-13.3
Test 4 Run 2	-13.5	-14.6	-1.9	-12.2	-21.1	-26.6	-12.8
Test 4 Run 1	-15.0	-16.4	-0.1	-13.5	-23.3	-25.7	-13.8
Test 3 Run 3	-14.4	-19.0	-2.3	-11.7	-23.8	-24.4	-13.5
Test 3 Run 2	-13.5	-18.8	-1.5	-12.0	-21.8	-25.6	-13.9
Test 3 Run 1	-16.4	-16.2	-1.3	-14.0	-20.5	-25.5	-11.8
Test 2 Run 3	-13.2	-19.3	-2.6	-9.1	-22.6	-28.5	-12.9
Test 2 Run 2	-16.0	-16.3	-0.9	-12.2	-22.7	-24.4	-12.0
Test 2 Run 1	-14.1	-10.8	0.0	-12.9	-25.8	-23.4	-12.6
Test 1 Run 3	-11.4	-14.7	-2.8	-10.9	-19.5	-22.2	-15.4
Test 1 Run 2	-12.7	-19.8	-2.4	-10.7	-23.4	-21.6	-13.9
Test 1 Run 1	-14.2	-21.7	-2.0	-4.2	-24.3	-20.5	-12.3
	Region 1	Region 2	Region 3	Region 4	Region 5	Region 6	Region 7

Figure 3-24: Heat map of the dataset for normalized microphone pressure level.

The dynamic pressure sensors also had some interesting behavior through the different test runs. It can be seen that region four is primarily the transition region for energy as the moves to the second modulating position. The inlet and outlet dynamic pressure power was close to even in region four for all tests. This shows that after the valve flows oil the pressures equalize causing the port dynamic pressure energy to be similar. But once the valve begins to close in region 5 the inlet port is closed not allowing any energy in the inlet port. But as the outlet pressure drops the energy is still prevalent in region 5. Another finding is that the rapid opening and closing of the valve causes outlet dynamic pressure energy to be spread across more regions compared to the slower valve sweeps. This could be due to the internal flow of the fluid having more turbulence when compared to the slower pedal press runs.

	Top Inlet Dynmaic Pressure Normalized dB						
Test 5 Run 3	-24.2	-15.9	-3.2	-5.3	-8.6	-12.2	-12.5
Test 5 Run 2	-25.1	-15.4	-1.8	-4.1	-5.8	-11.4	-11.3
Test 5 Run 1	-24.6	-11.9	-0.4	-3.1	-3.7	-8.9	-9.1
Test 4 Run 3	-25.3	-16.2	-4.1	-5.4	-12.1	-18.7	-20.0
Test 4 Run 2	-25.2	-14.8	-2.5	-4.1	-10.5	-16.5	-17.5
Test 4 Run 1	-25.6	-13.7	-1.4	-2.7	-16.5	-20.4	-21.7
Test 3 Run 3	-24.8	-15.9	-3.6	-5.5	-11.4	-15.5	-16.6
Test 3 Run 2	-24.8	-16.0	-1.9	-3.6	-9.2	-15.1	-15.3
Test 3 Run 1	-26.3	-13.9	-0.6	-2.5	-8.2	-12.9	-14.2
Test 2 Run 3	-24.7	-17.0	-3.1	-4.6	-7.5	-11.6	-11.3
Test 2 Run 2	-25.3	-15.5	-1.6	-4.4	-6.0	-10.4	-10.8
Test 2 Run 1	-24.8	-12.3	0.0	-2.6	-5.7	-7.6	-6.5
Test 1 Run 3	-23.7	-16.1	-2.7	-4.9	-12.0	-9.4	-6.2
Test 1 Run 2	-24.0	-16.7	-1.1	-3.1	-10.1	-7.7	-4.5
Test 1 Run 1	-25.0	-16.7	0.0	0.0	-4.6	-6.3	-3.1
	Region 1	Region 2	Region 3	Region 4	Region 5	Region 6	Region 7

Figure 3-25: Heat map of the dataset for normalized top inlet dynamic pressure level.

	Top Outlet Dynmaic Pressure Normalized dB						
Test 5 Run 3	-25.769	-17.877	-6.216	-2.746	-0.211	-5.091	-5.734
Test 5 Run 2	-26.790	-17.243	-6.423	-2.974	-0.259	-10.393	-6.882
Test 5 Run 1	-26.019	-16.973	-7.034	-2.412	0.000	-10.218	-7.316
Test 4 Run 3	-26.815	-18.064	-7.827	-4.082	-1.206	-9.617	-5.480
Test 4 Run 2	-26.680	-18.227	-7.918	-3.214	-1.162	-10.697	-5.530
Test 4 Run 1	-27.220	-18.047	-8.910	-4.354	-1.424	-6.487	-4.770
Test 3 Run 3	-26.622	-17.637	-6.957	-2.448	-0.776	-6.684	-5.118
Test 3 Run 2	-26.328	-17.640	-6.119	-2.045	-0.978	-11.428	-5.424
Test 3 Run 1	-27.927	-17.406	-7.170	-2.454	-0.594	-9.155	-5.275
Test 2 Run 3	-26.338	-17.877	-6.192	-1.897	-0.255	-5.244	-5.848
Test 2 Run 2	-27.391	-17.709	-6.141	-2.137	-0.221	-6.749	-6.007
Test 2 Run 1	-26.290	-16.229	-6.586	-2.755	-0.318	-1.741	-5.002
Test 1 Run 3	-25.252	-16.290	-3.724	-1.393	-1.821	-2.266	-5.854
Test 1 Run 2	-25.549	-17.913	-3.064	-1.251	-2.161	-0.637	-3.728
Test 1 Run 1	-26.460	-19.566	-4.769	-1.228	-1.015	-1.744	-3.172
	Region 1	Region 2	Region 3	Region 4	Region 5	Region 6	Region 7

Figure 3-26: Heat map of the dataset for normalized top outlet dynamic pressure level.

The final sensor analyzed with this method was the accelerometer mounted on the valve body. A strong correlation between the acceleration in the z-direction and the acoustic flow noise created was discovered when comparing the plots to each other. Both showed the highest normalized value for test 2 run one and also the second-highest value for test 4 run 1

	Accelerometer X Direction Normalized Acceleration dB						
Test 5 Run 3	-10.593	-10.536	-0.864	-7.301	-16.376	-17.316	-11.558
Test 5 Run 2	-11.498	-10.471	-0.168	-7.530	-15.426	-16.831	-10.561
Test 5 Run 1	-10.726	-7.239	-1.591	-7.938	-15.471	-17.046	-11.202
Test 4 Run 3	-11.610	-10.975	-2.662	-5.351	-15.084	-16.961	-11.065
Test 4 Run 2	-11.360	-9.289	-2.618	-6.657	-15.169	-16.743	-10.974
Test 4 Run 1	-11.876	-8.811	-2.250	-4.610	-16.090	-16.465	-11.208
Test 3 Run 3	-11.211	-11.214	-1.640	-10.320	-16.021	-17.335	-10.734
Test 3 Run 2	-10.895	-11.710	0.000	-7.117	-15.305	-16.048	-10.867
Test 3 Run 1	-12.651	-9.219	-2.424	-9.375	-15.797	-16.802	-10.250
Test 2 Run 3	-11.104	-12.732	-2.769	-8.626	-15.824	-17.407	-10.679
Test 2 Run 2	-12.208	-10.103	-0.392	-7.312	-15.927	-16.249	-10.280
Test 2 Run 1	-11.060	-8.825	-3.175	-12.182	-17.605	-15.384	-10.549
Test 1 Run 3	-9.937	-12.539	-3.382	-8.837	-17.296	-16.981	-11.739
Test 1 Run 2	-10.232	-14.454	-2.800	-7.588	-16.623	-15.243	-10.987
Test 1 Run 1	-11.179	-15.160	-3.807	-3.705	-16.528	-14.358	-10.158
	Region 1	Region 2	Region 3	Region 4	Region 5	Region 6	Region 7

Figure 3-27: Heat map of the dataset for normalized Acceleration X.

	Accelerometer Y Direction Normalized Acceleration dB						
Test 5 Run 3	-11.879	-9.785	-0.714	-8.885	-17.559	-19.011	-13.028
Test 5 Run 2	-12.737	-9.558	-0.010	-9.016	-16.332	-18.370	-11.852
Test 5 Run 1	-12.122	-6.162	0.000	-9.773	-15.944	-18.761	-12.552
Test 4 Run 3	-12.911	-10.585	-2.126	-7.138	-16.049	-18.155	-12.294
Test 4 Run 2	-12.757	-8.394	-1.475	-8.409	-16.495	-18.061	-12.212
Test 4 Run 1	-13.227	-8.132	-1.244	-6.710	-17.127	-17.706	-12.584
Test 3 Run 3	-12.578	-10.681	-2.013	-11.568	-17.351	-18.441	-12.031
Test 3 Run 2	-12.300	-10.732	-0.911	-9.133	-16.315	-17.522	-12.370
Test 3 Run 1	-13.943	-8.545	-1.503	-11.709	-17.184	-18.230	-11.751
Test 2 Run 3	-12.417	-11.995	-2.609	-10.288	-17.222	-18.761	-11.958
Test 2 Run 2	-13.654	-9.368	-1.402	-10.366	-16.957	-17.600	-11.606
Test 2 Run 1	-12.350	-9.718	-4.346	-13.571	-18.469	-15.230	-11.956
Test 1 Run 3	-11.294	-13.139	-5.160	-11.341	-18.292	-17.644	-13.017
Test 1 Run 2	-11.579	-15.141	-5.173	-10.005	-16.644	-15.342	-12.246
Test 1 Run 1	-12.550	-15.736	-5.492	-6.791	-17.899	-14.080	-11.592
	Region 1	Region 2	Region 3	Region 4	Region 5	Region 6	Region 7

Figure 3-28: Heat map of the dataset for normalized Acceleration Y.

	Accelerometer Z Direction Normalized Acceleration dB						
Test 5 Run 3	-17.875	-13.019	-3.485	-16.690	-23.574	-24.932	-18.982
Test 5 Run 2	-18.943	-12.864	-3.057	-16.826	-22.786	-24.189	-18.057
Test 5 Run 1	-18.149	-10.420	-2.165	-18.044	-22.670	-24.611	-18.589
Test 4 Run 3	-19.036	-13.223	-3.679	-15.103	-22.264	-24.238	-18.454
Test 4 Run 2	-18.852	-11.862	-2.954	-17.529	-22.616	-23.825	-18.484
Test 4 Run 1	-19.363	-11.702	-1.730	-14.443	-23.354	-23.792	-18.588
Test 3 Run 3	-18.721	-13.327	-3.724	-19.644	-23.456	-24.370	-18.324
Test 3 Run 2	-18.529	-13.172	-3.106	-16.951	-22.758	-23.189	-18.347
Test 3 Run 1	-19.808	-11.624	-2.270	-19.586	-22.977	-24.332	-17.758
Test 2 Run 3	-18.574	-13.853	-3.811	-15.552	-23.321	-24.574	-17.959
Test 2 Run 2	-19.443	-12.259	-2.892	-18.245	-23.154	-23.610	-17.732
Test 2 Run 1	-18.582	-6.760	0.000	-18.729	-24.811	-21.564	-18.102
Test 1 Run 3	-17.370	-8.611	-3.029	-17.698	-25.105	-23.500	-19.129
Test 1 Run 2	-17.652	-11.096	-2.523	-17.208	-24.435	-21.536	-18.453
Test 1 Run 1	-18.585	-12.105	-1.131	-11.289	-23.933	-20.713	-17.494
	Region 1	Region 2	Region 3	Region 4	Region 5	Region 6	Region 7

Figure 3-29: Heat map of the dataset for normalized Acceleration Z.

With all the testing concluded there were many impactful discoveries made about both valves tested under the scope of this research. The most significant findings were the identification of valve flow regions and the behavior of the valve spools during this excitation. Other findings were the identification of brake valve ports having different noise characteristics depending on pedal operation rate. Further analysis was also done using wavelet filters to isolate the hydraulic flow noise from other mechanical interference but due to time constraints was not included in the scope of this thesis. Moving forward these findings would be a great starting point to design and test prototype spool designs to lengthen the transition period as the valve cracks to allow flow.

4 Conclusion

The first part of this project was a continuation of work completed by the previous graduate student. With testing expanded, many of the earlier findings were validated by the new round of testing. However, other unknown parameters complicated the initial scope of work. This includes the compensator spool, which was initially assumed to have no impact on flow noise, seeing it did not interact with the flow during the spool opening. These assumptions were proven incorrect when it was discovered through new instrumentation that the compensator played a large part in regulating flow as the valve opened. The findings corroborated the previous research students' work even with these complications.

This includes finding the boundary conditions had little significance to the induced flow noise of the valve. Further research would not need to be as in-depth, allowing a diverse valve sweep test plan to be tested. Next, pump speed contributed to the creation of flow noise in the valve, meaning that the increased flow rate through the valve and design of a more significant pressure gradient in the valve directly correlated to the creation of flow noise. This finding is also supported by Cohen's work [2] and Cairns [13]. However, system backpressure did not impact the creation of flow noise in the operational range of 1000-2000 psi; the flow noise did increase as the backpressure dropped below 1000 psi.

When testing was conducted at 500 psi, there was a noticeable increase in flow noise, further supporting the findings that an increased pressure gradient inside the valve is a significant factor in determining the amount of flow noise during operation.

The final advancement was using hydraulic flow noise regions during the accessory valve testing. Trying to predict and characterize the flow behavior across the whole valve; was simplified by determining critical spool displacements that caused the flow to change behavior. For the accessory valve, the flow-induced noise started at 33% max displacement, and the flow would mature and decrease noise at 50% displacement.

During the second phase of the project, the scope of research moved away from the accessory valve and instead focused on the characterization of the brake valve. This phase yielded many results, allowing the brake valve's behavior to be better understood. The testing focused on determining how different brake pedal actuation speeds affected the valve's creation of hydraulic flow noise. With testing finished, key findings were discovering seven different flow regions regarding the brake spool displacement. It was also determined that the valve behaved similarly in the sound levels produced through all of the runs and did not depend on the pedal speed.

The valve behavior was easier to visualize through valve flow regions while also allowing power measurements to be calculated for each region. It was found that region three was the most significant contributor to flow noise with the brake spool at maximum displacement. Region three also contained nearly all of the flow through the valve, with the slack adjusters filling at this point. Ultimately it was determined that future research for vibration and acoustic energy creation should focus on this region, seeing as it was the most significant for that type of flow energy. Once the slack adjusters filled, the pressure would be at a maximum and the valve would start modulation to maintain that pressure. During this process, the inlet and outlet power for the dynamic pressure sensors would be close to equal, meaning this region was known as the transition region. After this, the valve would begin to close in region five, creating large spikes in the outlet dynamic pressure energy; however, this did not correlate to an increase in acoustic flow noise. It was determined that flow moving from very high to lower pressures through the valve body was the most significant contributor to flow noise. This sensor showed a similar trend with high valve body acceleration translating closely to the creation of audible flow noise.

Next, the valve ports showed unique behavior through the testing, with dynamic pressure responses changing depending on the pedal operation. It was found that run 2 test 1 created the most audible flow noise and the most considerable vibration input to the structure. This finding was exciting because it also acted as

a transition in valve behavior between the faster runs of tests one and two to the slower runs of tests 3-7. Many of the unique characteristics that evolved through testing seemed to be separated into these categories. This included the characterization of the mechanical clunk, which was the settling of the spool across the end of region three and into region four. This clunk was a predominant feature in tests one and two spectrograms but faded in energy as the braking operation took longer.

This research will benefit the development of new brake spool designs; this research has shown that much of the acoustic flow noise generated by the valve only occurs during a small time in the valve operation. Future work on this project could include studying the transmissibility of energy from the valve to the structure. This boundary condition could then be modified to isolate the valve's energy from entering the cabin. Furthermore, using models could further validate the research and create a computational system that would predict the creation of flow noise based on input variables.

5 Reference List

[1] Kolb, Ben, et al. “Experimental Characterization of Hydraulic System Sound.”

Michigan Technological University, 2019.

[2] Cohen, Zachary, et al. “Experimental Characterization of Spool Valve Flow Noise.”

Michigan Technological University, 2020.

[3] Skaistis, Stan. *Noise Control of Hydraulic Machinery*. Marcel Dekker, 1988.

[4] Elsheikh, M.M, et al. “A Numerical and Experimental Investigation of Flow Induced Noise In Hydraulic Counterbalance Valves” University of South Florida, 2015

[5] TechTrixInfo. *How piston pump works*. YouTube,

<https://www.youtube.com/watch?v=BEpQFZ5BG8c>

[6] Zhiwei Hu, Christopher L Morfey, and Neil D Sandham. Sound radiation from

a turbulent boundary layer. *Physics of fluids* (1994), 18(9), 2006.

[7] “Piston pump: Working, types, advantages and disadvantages,” *ElProCus*, 18-Jun-2019. [Online]. Available: <https://www.elprocus.com/piston-pump-working-and-different-types/>. [Accessed: 15-Feb-2022].

[8] “Hydraulic axial piston pumps,” *Hydraulic Pump*, 29-Jul-2019. [Online]. Available: <http://www.hydraulic-pump.info/hydraulic-engineering/hydraulic-axial-piston-pumps.html>. [Accessed: 15-Feb-2022].

[9] Hydraulic fluid power — Determination of pressure ripple levels generated in systems and components — Part 1: Method for determining source flow ripple and source impedance of pumps. Standard, International Organization for Standardization, October 2015.

[10] K A Edge and T J Wing. The measurement of the fluid borne pressure ripple characteristic of hydraulic components. Proceedings of the Institution of Mechanical Engineers, Part B: Management and engineering manufacture, 197 Issue 4:247–254, 1983.

[11] *Occupational noise exposure*, vol. Occupational Safety and Health Standards. 1981.

[12] J. Blackburn, J Coakley, and F Ezekiel. “Transient forces and valve instability” in Fluid Power Control. The Technology Press of M.I.T., 1960.

[13] C. Cairns, R. J. Whitson, P. Strachan, and M. Wheel. Prediction of noise generated by orifice plates in liquid systems using a modified form of iec 534-8-4:1994. Advances in Fluid Mechanics III, 29:675–686, 2000.